High-Throughput Analysis of Lung Immune Cells in a Murine Model of Rheumatoid Arthritis-Associated Lung Disease

Authors: Rohit Gaurav, MSc, PhD[1], Ted R. Mikuls, MD, MSPH[2,3], Geoffrey M. Thiele, PhD[2,3], Amy J. Nelson, MT (ASCP)[1], Meng Niu, PhD[5], Chittibabu Guda, PhD[5], James D. Eudy, PhD[5], Austin E. Barry BS[1], Todd A. Wyatt, PhD[2,4,6], Debra J. Romberger, MD[2,4], Michael J. Duryee, MS [2,3], Bryant R. England, MD, PhD [2,3], Jill A. Poole, MD[1]

[1]Division of Allergy and Immunology, Department of Internal Medicine, University of Nebraska Medical Center (UNMC); [2]Veterans Affairs Nebraska-Western Iowa Health Care System, Research Service, Omaha, NE; [3]Division of Rheumatology & Immunology; [4]Division of Pulmonary, Critical Care & Sleep, Department of Internal Medicine, UNMC; [5]Department of Genetics, Cell Biology and Anatomy, UNMC; [6]Department of Environmental, Agricultural & Occupational Health, College of Public Health, UNMC, Omaha, Nebraska 68168, USA

Corresponding Author:

Rohit Gaurav, MSc, PhD, FAAAAI
Division of Allergy and Immunology
Department of Internal Medicine
University of Nebraska Medical Center
985910 Nebraska Medicine
Omaha, NE 68198-5910
Email: rohit.gaurav@unmc.edu

Short title: RNA sequencing identifies unique cell populations in RA-related lung disease

Abstract

Rheumatoid arthritis (RA)-associated lung disease is a leading cause of mortality in RA, yet the mechanisms linking lung disease and RA remain unknown. Using an established murine model of RA-associated lung disease combining collagen-induced arthritis (CIA) with organic dust extract (ODE)-induced airway inflammation, differences among lung immune cell populations were analyzed by single cell RNA-sequencing. Additionally, four lung myeloid-derived immune cell populations including macrophages, monocytes/macrophages, monocytes, and neutrophils were isolated by fluorescence cell sorting and gene expression was determined by NanoString analysis. Unsupervised clustering revealed 14 discrete clusters among Sham, CIA, ODE, and CIA+ODE treatment groups: 3 neutrophils (inflammatory, resident/transitional, autoreactive/suppressor), 5 macrophages (airspace, differentiating/recruited, recruited, resident/interstitial, and proliferative airspace), 2 T-cells (differentiating and effector), and a single cluster each of inflammatory monocytes, dendritic cells, B-cells and natural killer cells. Inflammatory monocytes, autoreactive/suppressor neutrophils, and recruited/differentiating macrophages were predominant with arthritis induction (CIA and CIA+ODE). By specific lung cell isolation, several interferon-related and autoimmune genes were disproportionately expressed among CIA and CIA+ODE (e.g. *Oasl1*, *Oas2*, *Ifit3*, *Gbp2*, *Ifi44*, and *Zbp1*), corresponding to RA and RA-associated lung disease. Monocytic myeloid-derived suppressor cells were reduced, while complement genes (e.g. *C1s1* and *Cfb*) were uniquely increased in CIA+ODE mice across cell populations. Recruited and inflammatory macrophages/monocytes and neutrophils expressing interferon-, autoimmune-, and complement-related genes might contribute towards pro-fibrotic inflammatory lung responses following airborne biohazard exposures in setting of autoimmune arthritis and could be predictive and/or targeted to reduce disease burden.

50 **Keywords**: rheumatoid arthritis, lung disease, myeloid-derived immune cell populations, RNA

51 sequencing

52

Introduction

Several lung diseases have been associated with rheumatoid arthritis (RA), including interstitial lung disease (ILD), chronic obstructive pulmonary disease (COPD), pulmonary nodules, pleural effusions, bronchiolitis obliterans, and asthma (1-3). Affecting up to 40% or more of RA patients, RA-associated lung diseases pose a substantial burden to healthcare systems because of the increased morbidity and mortality, decreased quality of life, and tremendous healthcare costs (2, 4, 5). Evidence of RA-related autoantibodies generated in lung mucosa, even in the absence of articular manifestations of RA (6), as well as increased concentrations of serum anti-citrullinated protein antibody accompanying RA-related lung diseases (1, 4, 7), reinforces the pathogenic links between pulmonary inflammation and autoimmunity leading to the development of RA. Therapeutic option for RA-associated lung disease are limited (8), and key cellular and/or mediators predictive of the development and/or progression of RA-associated lung disease are lacking (9). Thus, studies are warranted to investigate and identify precise mechanisms underpinning these associations.

Exposure to environmental factors such as cigarette smoke represent shared risk factors in the development of RA and inflammatory lung diseases (3, 10). However, insight into how inhalant injury might lead to or exacerbate RA and its pulmonary manifestations, has been limited in the absence of a relevant disease model. Recently a pre-clinical animal model to provide insight into the important cellular players and decipher molecular and potential mechanistic pathways involved in RA-associated inflammatory lung disease was established (11). Specifically, the combination of the collagen-induced arthritis (CIA) model with a model of airborne biohazard exposure (e.g. organic dust extract/ODE) resulted in augmented arthritis, increased systemic autoimmunity, and promotion of pre-fibrotic inflammatory lung changes in mice (11) consistent with RA-associated

lung disease pathophysiology. However, the mechanisms underlying these observations are not known. Here, we hypothesized that RA-associated lung disease is associated with unique cellular phenotypes and specific novel gene expression of *in vivo* exposed lungs. Leveraging this novel murine model, single-cell RNA sequencing (scRNA-seq) and unsupervised clustering were applied to lung immune cells among Sham, CIA, ODE, and CIA+ODE treatment groups to explore exposure-related differences in cellular subsets, transcriptional profiles, and associated biologic pathways. In separate complimentary studies to confirm key scRNA-seq findings, lung myeloid-derived cells (i.e. monocytes/macrophages and granulocytes) were isolated and subjected to gene-expression analysis.

Materials and methods

Animals

Arthritis prone DBA/1J male mice between 6-8 weeks of age were purchased from Jackson Laboratory (Bar Harbor, ME, USA) and fed alfalfa-free chow *ad libitum* (Envigo Teklad, Huntingdon, Cambridgeshire, UK) as per supplier recommendations. All animal procedures were approved by the UNMC Institutional Animal Care and Use Committee (protocol #19-043-05) and were in accordance with NIH guidelines for the use of rodents.

Organic dust extract

Organic dust extract (ODE) was prepared as previously reported (12) to model airway inflammatory disease. Briefly, an aqueous extract of organic dust from swine confinement feeding facilities (microbial-enriched agriculture setting) was prepared by incubating 1 g dust in 10 ml sterile Hank's Balanced Salt Solution (Mediatech, Manassas, VA, USA) for 1 hour at room

temperature followed by centrifugation for 10 minutes at 2,850 x g and repeated twice. The end supernate was filter-sterilized with a 0.22 μm syringe filter to remove any microorganisms and coarse particles. Constituents of the extract have been well characterized and include both endotoxin and peptidoglycans (11, 12). ODE stock was prepared and stored at –20˚C in batches; aliquots were diluted for each experiment to a final concentration (vol/vol) of 12.5% in sterile phosphate buffered saline (PBS; pH = 7.4). Endotoxin concentrations ranged from 150-175 EU/mL as determined using the limulus amebocyte lysate assay (Lonza, Walkersville, MD, USA). This concentration of ODE has been previously shown to produce optimal experimental effects and is well-tolerated in mice (11, 12).

Animal co-exposure model

The protocol for the co-exposure model has been previously described (11). Briefly, mice were age-matched and randomized to 4 treatment groups: Sham (saline injection, saline inhalation), collagen-induced arthritis (CIA; CIA injection, saline inhalation), ODE (saline injection, ODE inhalation), and CIA + ODE (CIA injection, ODE inhalation). CIA was induced with two subcutaneous tail injections (100 μg) of chick type II collagen (2 mg/ml) emulsified in Freund's complete adjuvant (FCA) on day 1 and in Freund's incomplete adjuvant (IFA) on day 21. Sham injections and saline inhalation were conducted with sterile PBS. Following an established protocol, 50 μl of intranasal saline or 12.5% ODE daily for 5 weeks (weekends excluded) was used to induce airway inflammatory disease (11, 12).

Single-cell RNA sequencing

Mice were euthanized with isoflurane in a desiccator. Tracheostomy was performed for cannula insertion. Lungs were exposed from the thoracic cavity and perfused with 10 ml heparin-PBS (11). Harvested lungs were dissociated with gentleMACS dissociator (Miltenyi Biotech,

Auburn, CA, USA) in a digestion solution (collagenase I, 0.2 µg/µl + DNase I, 75 U/ml + heparin, 1.5 U/ml, in Dulbecco's Modified Eagle's Media; DMEM) and incubated for 30 minutes at 37 °C in a shaking incubator. Digestion solution activity was neutralized with PBS containing 4 mM EDTA. Red blood cells were lysed with 1 ml ammonium-chloride-potassium (ACK) lysis buffer (Quality Biological, Gaithersburg, MD, USA) for 1 minute and neutralized with ice-cold DMEM (Gibco). Cells were processed for RNAseq in FACS buffer (2% fetal bovine serum (FBS) + 0.1% NaN_3 in PBS). All reagents purchased from Sigma unless otherwise specified.

Single cell suspensions generated from whole lung were quantified and viability tested using a LUNA-FL™ Dual Fluorescence Cell Counter (Logos Biosystems, Annandale, VA, USA). Single cells were then isolated from cell suspensions (100-2,000 cells/µl) using a 10x Chromium controller per manufacturer's suggested protocol (10x Genomics, Pleasanton, CA). Following cell capture, the gel beads in emulsion (GEM)/sample solution was recovered and placed into strip tubes. Reverse transcription was performed on a thermocycler (C1000 Touch™ Thermal Cycler, Bio-Rad, Hercules, CA, USA) per recommended protocol followed by cDNA amplification. Amplified products were solid phase reversible immobilization (SPRI) bead-purified and evaluated by Fragment Analyzer (Agilent, Santa Clara, CA, USA). Twenty-five percent of the cDNA volume was subjected to fragmentation and double-sided SPRIselect (Beckman Coulter, Indianapolis, IN, USA) was used for PCR purification and clean-up. After adaptor ligation, SPRI clean-up was performed and PCR amplification using sample specific indexes for each sample was completed. PCR products were purified, quantified and library size distribution determined by Fragment Analyzer. Libraries were sequenced per the manufacturer's suggested parameters on a NextSeq500 sequencer to an average depth of 50,000 reads per cell.

Single-cell RNA sequencing data processing

Basecall files (BCL) were generated through 10xGenomics Chromium Single cell 3' Solution followed by RNA Sequencing using Nextseq 500 and Nextseq 550. *Cellranger mkfastq* was used for demultiplexing and to convert BCL files into FASTQ files. FASTQ files were run through *Cellranger count* to perform alignment (using STAR aligner), filtering, and unique molecular identifier (UMI) counting. Chromium cellular barcodes were used to generate gene-barcode matrices, perform clustering, and do gene expression analyses. *Cellranger aggr* was used to normalize and pool the results from different samples, followed by the application of Principal Components Analysis (PCA) to change the dimensionality of the datasets. t-SNE (t-Stochastic Neighbor Embedding) was used to visualize the data in a 2-D space. Graph-based unsupervised clustering was then used to cluster the cells. We used Loupe browser (13), R packages including cellranger R-kit (14), complex heatmap (15), and Geom_violin (16) for more in-depth analysis to compare genes expression in each cluster compared to all the other clusters and plot the data. The data sets have been deposited to the Gene Expression Omnibus (GEO) database with access number GSE155436.

Lung cell sorting

In separate studies, following mouse euthanasia and lung perfusion, lungs were inflated with 1 ml digestion solution/mouse containing 0.5 mg/ml Liberase™ (medium Thermolysin concentration; Millipore Sigma, St. Louis, MO, USA) and 235.5 U/ml DNAse I in Hank's Balanced Salt Solution (pH=7.2). Inflated lungs were dissociated with gentleMACS dissociator (Miltenyi Biotech, Auburn, CA, USA) and incubated for 15 minutes at 37 °C in a shaking incubator. Digestion solution activity was neutralized with FA3 buffer (10mM HEPES, 2mM EDTA, 1% FBS in PBS). The single cell lung suspensions were incubated with CD16/32 (Fc Block BD Biosciences, San Jose, CA) to minimize nonspecific antibody staining. Next, cells stained with

mAbs directed against rat anti-mouse CD45 (clone 30-F11), Ly6C (clone AL-21), Ly6G (clone 1A8), CD11b (clone M1/70), and hamster anti-mouse CD11c (clone N418), and live/dead fixable blue dead cell stain kit (Invitrogen, Eugene, OR, USA) . Antibodies to CD45 were obtained from eBiosciences (Santa Clara, CA, USA); CD11b and Ly6G from BioLegend (San Diego, CA, USA); CD11c from Invitrogen, and the remainder from BD Biosciences. Flow-sorting was done with FACSAria II (BD Biosciences). Live $CD45^+$ singlets were gated on $Ly6C^+Ly6G^+$ to sort neutrophils. Lymphocytes (based on FSC and SSC) and neutrophils (based on Ly6C and Ly6G staining) were then reverse gated to further select for 3 monocyte/macrophage populations: macrophage ($CD11c^{high}$, $CD11b^{variable}$), monocytes-macrophages ($CD11c^{intermediate}$,$CD11b^{high}$), and monocytes ($CD11c^{-}$, $CD11b^{high}$).

RNA isolation

The 4 cell-sorted populations were counted, assessed for viability by trypan blue exclusion (>95%), washed and lysed with RLT buffer containing β-mercaptoethanol for RNA isolation as per manufacturer's instructions with Qiagen RNAeasy Micro Kit (Qiagen, Germantown, MD, USA).

NanoString nCounter system

Quality and quantity of total RNA was evaluated using a Fragment Analyzer (Agilent, Santa Clara, CA, USA) and Nanodrop (ThermoFisher), respectively. Total RNA (25-50 ng) was hybridized and processed per the manufacturer's suggested protocol with capture and reporter probes to prepare target-probe complexes using reagents from the Mouse Autoimmune profiling panel containing 771 genes (NanoString, Seattle, WA, USA). Complexes were purified, immobilized and aligned on a cartridge for counting on the nCounter system and processed as per the manufacturer's instructions.

For NanoString analyses, three independent studies of 2-3 pooled mice per group/experiment (N=3) were analyzed by two-way ANOVA with Tukey's multiple comparisons test. Gene expression data were normalized to 20 housekeeping genes, treatment groups (CIA, ODE and CIA+ODE) were compared to Sham, and data plotted as fold-change. One-way ANOVA with Tukey's multiple comparison test was used on myeloid-derived suppressor cell (MDSC) posthoc analysis. Bar graphs were used to depict means with standard errors of the ratio change in MDSCs normalized to Sham (percentile of MDSC treatment group divided by percentile of MDSC Sham group). Statistical analyses were performed using the GraphPad Prism software, version 8.4.3 (GraphPad, San Diego, CA), and statistical significance accepted at p-values <0.05.

Results

ScRNA-seq identifies 14 unique immune cell subsets

The 10x genomics platform was utilized to cumulatively capture all lung cells. In total, 16,822 cells were analyzed with a mean of 42,901 post-normalization reads per cell and 956 median genes per cell. Unsupervised clustering was performed on 11,577 $CD45^+$ cells and plotted on *t*-distributed Stochastic Neighbor Embedding (t-SNE). Projection of cells was colored based on unique molecular identifier (UMI) count to identify level of transcripts among the cells. The average UMI count range was roughly between 2,000 to 12,000. Cells that were distributed in the middle showed the highest level of transcripts while cells at the top showed the lowest level (Figure 1A). Unsupervised clustering on the t-SNE projected cells revealed 14 unique immune cell subsets coded by different colors and arbitrary numbers (Figure 1B). Clusters 3, 4 and 8 were identified as neutrophil subsets based on distribution of *Csf3r* (granulocyte colony stimulating factor receptor (17)) in t-SNE analysis. (Figure 1C). Macrophages were distributed in the middle and were

identified with *Cd11c* (ITGAX) expression in clusters 1, 2, 5, 11, 14, and partially in cluster 10. Monocytes (inflammatory monocytes) were identified with *F13a1* expression in cluster 12. Cluster 9 showed high levels of *Ccl5* expression suggesting the presence of NK cells. Similarly, *Cd19* expressing cells in cluster 7 identified B lymphocytes, and *Trbc2* expression in clusters 6 and 13 identified T lymphocytes, along with expression in the NK cell population (cluster 9). Dendritic cells (DCs) were located in cluster 10 and were characterized by *Siglech* expression, particularly evident in cluster 10a (Figure 1C).

CIA and ODE drive unique distributions of immune cells within identified clusters

The 4 treatment groups (Sham, CIA, ODE, and CIA+ODE) exhibited unique distributions of lung immune cells among the identified clusters (Figure 2A-B). Among the neutrophil clusters, Sham was exclusively represented by cluster 4, but not cluster 3 or 8. In contrast, the CIA group almost entirely showed neutrophil distribution in cluster 3. The ODE group demonstrated selective distribution of neutrophils in cluster 8 with overlap into cluster 4. In the combination exposure CIA+ODE group, there was broader distribution of neutrophils with predominance in cluster 3, but also evidence for distribution in cluster 4 and partially in cluster 8 (Figure 2A-B).

Among the macrophage clusters, the ODE group had prevalence in clusters 5, 1b and 1c compared to the CIA group. Likewise, the ODE group lacked clusters 1a and 2a. A subset of cluster 12 (12b) and cluster 10 (10b) were unique to the CIA group, while clusters 10a and 12a were unique to the ODE group. The combination group with CIA+ODE showed a mixed population representing CIA and ODE, while leaning more towards the CIA group (Figure 2A-B).

Lymphocyte populations were confined to clusters 6, 7, 9, and 13, and were represented in all treatment groups, although modest shifts in cell population distribution were observed.

Particularly, NK cells (cluster 9) and B cells (cluster 7) were differentially expressed in ODE and CIA treatment groups with apparent shifts from cluster 9a in ODE to cluster 9b in CIA and shifts from cluster 7a in ODE to cluster 7b in CIA, respectively. Similar to the macrophage clusters, the CIA+ODE group portrayed CIA and ODE group while inclining more towards the CIA group (Figure 2A-B).

Three distinct neutrophil populations revealed by scRNA-seq among treatment groups

Unsupervised clustering segregated 3 populations of granulocytes/neutrophils that were marked by unique gene expression (Figure 3A). Relative gene-expression compared to all other cell populations as log2 fold-change was plotted in a heat map (Figure 3B) and violin plot (Figure 3C) to compare transcript levels as well as cell distributions at different expression levels. Cluster 8 showed increased expression of inflammatory genes such as *Ccl3*, *Ccl4*, *Cxcl2*, *Upp1* and *Marcks1* (log2 fold-change range: 4.98-6.35), which are genes commonly upregulated in activated neutrophils (Figure 3B-C, and S1 Table) (18-22). Moreover, cluster 8 was exclusive to the ODE group. In contrast, cluster 3 exhibited increased expression of genes associated with immunosuppression and autoreactivity as well as genes that are characteristic of granulocytic MDSC (gMDSC) such as *S100a8*, *S100a9*, *Mmp8*, *Ifit3b*, *Ifit3*, *Cd33*, *Cd52* and *Stfa2l1* (log2 fold-change range: 5.16-6.03) (Figure 3B-C, and S1 Table) (23-29). Based on the gene expression profiles, cluster 8 was identified as "inflammatory neutrophils" and cluster 3 was identified as "gMDSC/autoreactive neutrophils". Intermediate to the two cell subsets, another neutrophil subset (cluster 4) was identified as resident/transitional neutrophils. This population of neutrophils (Figure 3, B-C, and S1 Table) demonstrated increased expression of *Csf3r*, *Il1r2*, *Slc40a1*, *Cxcr2*, and *Lmnb1* genes (log2 fold-change range: 3.91-4.24) that are required in neutrophil differentiation

and trafficking (17, 30-35). Neutrophils in the CIA+ODE group was distributed more like the CIA than the ODE group with predominant segregation in clusters 3 and 4 (Figure 2).

Signature genes were selected to highlight respective neutrophil populations on the t-SNE plot (Figure 3D). *Ccl3* was selected to highlight "inflammatory neutrophil" as *Ccl3* enhances recruitment and activation of neutrophils in a paracrine fashion (18, 19). Because *Il1r2* gene encodes for type 2 interleukin-1 receptor and is constitutively expressed in mouse neutrophils (30), it identified all subsets of neutrophils in the t-SNE clusters (Figure 3D). Autoreactive neutrophils/gMDSCs were exclusively positive for *Mmp8* and *Ifit3* in t-SNE. *Mmp8* is a neutrophil collagenase (36, 37) and *Ifit3* codes for interferon induced protein with tetratricopeptide repeats 3, as both are highly upregulated in gMDSCs and can suppress immune response (26, 27).

Identification of unique macrophage/monocyte/DC populations

Based on gene expression patterns among segregated populations found with unsupervised clustering, 5 discrete macrophage clusters, 1 inflammatory monocyte cluster, and 1 DC cluster were identified (Figure 4A). Cluster 1 was termed "airspace macrophages" based on increased expression (log2 fold-change range: 1.52-1.98) of *Ear1*, *Ear2*, *Ltc4s*, *Fabp1* and *Lyz2* compared to other clusters (Figure 4B-D), representing genes responsible for metabolism and inflammation/resolution (38-42) (S2 Table). Cluster 2 was labeled as "differentiating/recruited macrophages" as this cluster exhibited the highest expression (log2 fold-change range: 1.27-1.54) of *Net1*, *Tcf7l2*, *Abcg1*, *Pla2g15* and *Mrc1* representing genes implicated in differentiation, antigen uptake, and macrophage recruitment (43-47) (Figure 4B-D). Cluster 2 macrophages expressed genes associated with alternatively activated macrophages (M2 macrophages) (44, 47), and upregulate pathways for lipoprotein metabolism and redox signaling (S2 Table). Cluster 5 was identified as "recruited macrophages" based on the disproportionate expression (log2 fold-change

range: 1.5-1.96) of *Inhba*, *Cxcl3*, *Hmox1*, *Tgm2*, and *Car4* (Figure 4B-D). Cluster 5 was heterogeneous with *Inhba* representing classically activated (M1) macrophages or *Hmox1* as M2 macrophages, and also included genes that are involved in inflammation, adipogenesis, homeostasis and phagocytosis (48-57) (S2 Table).

Sham, CIA and CIA+ODE groups showed similar distribution of airspace (particularly cluster 1a) and recruited macrophages (especially cluster 2a) while the ODE group had a substantial reduction in these macrophage populations with segregation towards the center of the t-SNE plot in clusters 1b and 1c (Figure 2).

Cluster 11 was designated as "resident interstitial macrophages" with high transcript levels of *Apoe*, *Ccl2* and complement genes such as *C1qc*, *C1qb* and *C1qa* (Figure 4B-D) ranging from log2 fold-change of 3.54-3.91. This population also displayed heterogeneity with expression of both M1 and M2 genes (42, 58-62) involved in inflammation and resolution (S2 Table). Resident interstitial macrophages were more evident in the ODE compared to other treatment groups (Figure 2).

As reported by Mould *et. al.* (63), we also identified a distinct cluster of macrophages (cluster 14) with very high expression of proliferative and mitotic genes (log2 fold-change range: 5.79-8.12) including *Nusap1*, *Top2a*, *Birc5*, *Pclaf*, and *Mki67* (Figure 4B, 4C and 4D), which were termed "proliferative airspace macrophages." The upregulated pathways included cell-cycle, mitosis or proliferation-related pathways (S2Table) (63-65). These proliferative airspace macrophages were represented largely by the ODE and CIA+ODE groups (Figure 2).

Cluster 12 represented a unique cell population identified as "inflammatory monocytes." This population exhibited increased expression of *F13a1*, *Ms4a4c*, *Ly6c2*, *Plac8* and *Ccr2* (Figure 4B-D) (log2 fold-change range: 4.65-6.53), all characteristically expressed in inflammatory

307 monocytes and often correlated with anti-viral and/or autoimmune responses (66-74). Although
308 CIA+ODE group had a pronounced cluster 12, 12b represented the CIA group and ODE group
309 exhibited cluster 12a (Figure 2). A cell population in cluster 10 was identified demonstrating
310 elevated expression in genes (log2 fold-change range: 2.61-6.48) of *Siglech*, *Tcf4*, *Rnase6*, *Pou2f2*
311 and *Bst2* (Figure 4, B-D), which are distinctive of DCs (75-81). This population demonstrated
312 characteristics of plasmacytoid DCs involving genes associated with innate immunity and anti-
313 inflammatory pathways. The DC predominated with ODE and CIA+ODE groups in cluster 10a,
314 whereas cluster 10b predominated with Sham (Figure 2). Overall, CIA+ODE group distribution
315 of monocyte-macrophages followed neutrophils with overrepresentation of CIA group (Figure 2).

316 ## Lymphocytes segregate in four clusters among treatment groups

317 Four discrete lymphocyte clusters were found in the analysis (Figure 5A). Cluster 6 was
318 identified as "T lymphocytes", with increased expression (log2 fold-change range: 4.87-7.04) of
319 *Lef1*, *Igfbp4*, *Tcf7*, *Cd3d*, and *Cd3e* (Figure 5, B-D). This population favored type 2 $CD4^+$ cells
320 based upon the expression of differentiating or expanding population of T lymphocytic genes (82-
321 86). Cluster 6a was more represented by Sham whereas cluster 6b was represented by CIA and
322 CIA+ODE treatment groups. The ODE group had sparse distribution between cluster 6a and 6b
323 (Figure 2). In contrast to cluster 6, cluster 13 exhibited increased expression of genes indicative of
324 activated T lymphocytes including *Icos*, *Thy1*, *Cd3g*, *Ikzf2* and *Maf* (log2 fold-change range: 4.87-
325 5.87) and thus were termed as "effector T lymphocytes" (Figure 5, B-D) with upregulation of co-
326 stimulatory and adaptive immune pathways. Subtle differences were observed in the distribution
327 of activated T lymphocytes among the treatment groups (Figure 2).

328 Cluster 7 was remarkable for increased gene expression characteristic of B lymphocytes such
329 as *Ebf1*, *Cd79a*, *Ms4a1*, *Cd79b* and *Ighd* (log2 fold-change range: 7.29-7.77) (Figure 5B-D).

Along with genes implicated in B-cell differentiation, memory, signaling and autoimmunity, this cluster showed striking similarities with upregulated pathways in the T lymphocyte population (S3 Table) (87-90). B lymphocytes had an overall distribution in CIA+ODE group, but largely represented as cluster 7b in the CIA group. The ODE group had very few B lymphocytes with sparse distribution (Figure 2).

NK cell-specific gene expression was increased in cluster 9 with *Ncr1*, *Ccl5*, *Gzma*, *Nkg7* and *Prf1* (Figure 5, B-D) ranging from 7.83 to 7.87 log2 fold-change (S3 Table). These genes and pathways were predominately related to NK cell recruitment, activation and effector function (91-96). The Sham and ODE groups were represented by cluster 9a while the CIA group had more of cluster 9b. The CIA+ODE group had 9a and 9b clusters (Figure 2).

Differential gene expression of ex vivo sorted lung neutrophils across treatment groups represent disease progression

To understand the relevance of myeloid-derived lung cells in RA and RA-associated lung disease, these studies sought to determine whether gene expression of sorted lung myeloid-derived cells corresponded to disease-specific findings among treatment groups. Lung neutrophils were isolated by fluorescence activated cell sorting (FACS) based on traditional cell surface markers as $Ly6C^{+}$ $Ly6G^{high}$ cells (Figure 6A, gating strategy). By NanoString analysis, upregulated genes of isolated neutrophils resembled the gene expression demonstrated in scRNA-seq data by respective treatment groups. Neutrophils isolated from lungs of CIA and CIA+ODE groups (as compared to Sham) demonstrated increased transcript levels of genes involved in autoimmunity as well as genes associated with gMDSCs/autoreactive neutrophils. These included (CIA and CIA+ODE): *Ifit3* (21.7 and 7.49-fold), *Ifit1* (17.2 and 5.9-fold), *Oas2* (17.0 and 6.0-fold), *Zbp1* (14.6 and 8.5-fold), *Cxcl9* (5.1 and 8.5-fold), and *Oas1a* (12.5 and 7.2-fold) (Figure 6B and 6C). Interestingly, the

CIA+ODE group also showed gene expression that paralleled that of the ODE group, including increased transcript levels of *Src* (CIA+ODE: 6.1-fold and ODE: 7-fold), *Pf4* (7.7 and 5.3-fold), and complement cascade genes such as *C2* (9.6 and 6-fold-change), and *Cfb* (9.2 and 2.5-fold-change) (Figure 6B and 6C). In contrast, the ODE group demonstrated exclusive upregulation of *Ltf* (4.7-fold-change), *Ccl4* (3.2-fold), *Ccl3* (2.8-fold) and *Il1rn* (2.5-fold) as compared to Sham, consistent with the inflammatory neutrophil cluster (Figure 6B-C). There was a single complement cascade gene (*C1s1*) that was exclusively upregulated in CIA+ODE (4.3-fold) (Figure 6C).

Macrophage and monocyte populations from CIA and CIA+ODE groups exhibit gene profiles comparable to RA and RA-associated lung disease, respectively

After excluding lymphocytes and neutrophils, 3 separate lung monocyte-macrophage populations were sorted based upon CD11c and CD11b expression (S1 Figure and Figure 7A). These 3 populations are 1) $CD11c^{high}CD11b^{variable}$ macrophages, 2) $CD11c^{intermediate}CD11b^{high}$ mono-macs and 3) $CD11b^{high}CD11c^{-}$ monocytes. Of the $CD11c^{high}$ macrophages, the expression of CD11b (evident on the pseudocolor plots; Figure 7A) shifts to the right: CIA+ODE>ODE>CIA as compared to Sham. Increasing expression of CD11b on CD11c+ macrophages suggest an activated phenotype (97). Similar to neutrophils, the isolated macrophage population also demonstrated increased gene expression in CIA and CIA+ODE group that included *C1qb* (8.6 and 8.2-fold), *Cxcl9* (10.9 and 6-fold), *C1qa* (7.5 and 7.6-fold), *Ifi44l* (3.6 and 3.2-fold), *Cmklr1* (2.1 and 9.3-fold), *Ccl8* (3.2 and 7.6-fold), *Sdc1* (2.3 and 7.8-fold), and *Ms4a4a* (3.8 and 5.3-fold). Increased expression of *Gzma* was unique to the CIA group (6-fold) (Figure 7B-C), while *C1s1* was upregulated in both CIA+ODE (6.5-fold) and ODE (3-fold) groups along with *Pf4* (7.9 and 7.3-fold), *Itgam* (4.2 and 5.4-fold), and *Pdpn* (4 and 4.2-fold). Expression of *Src* (4.7, 5.6 and 6.4-

fold) and *Blnk* (2.3, 5.1 and 5.9-fold) was increased in all treatment groups (CIA, ODE and CIA+ODE) as compared to Sham (Figure 7, B-C).

The $CD11c^{intermediate}CD11b^{+}$ monocyte-macrophage population demonstrated increased expression of several interferon-associated and other genes implicated in autoimmune responses in CIA and CIA+ODE groups including *Gbp2* (7.4 and 6.9-fold), *Zbp1* (7 and 2-fold), *Ifi44* (6.6 and 4.3-fold), *Ifi44l* (6 and 5.1-fold), *Cxcl9* (5.8 and 8.1-fold), and *Fcgr1* (2.4 and 2.9-fold). ODE and CIA+ODE groups demonstrated increased expression of *Cxcl5* (3.4 and 2.6-fold), *Pdpn* (4.2 and 3.3-fold), *Pf4* (5.4 and 3.8-fold), and *Cxcl13* (6.8 and 3.6-fold) compared to Sham (Figure 8A-B). *Cfb* (5.9, 4.1, and 16.3-fold), *Ccl8* (11.3, 5.1, and 6.7-fold), and *C1s1* (5.8, 7, and 19.3-fold) were overexpressed in CIA, ODE and CIA+ODE groups, respectively, compared to Sham. Expression of non-canonical I-kappa-B kinase, *Ikbke*, associated with anti-viral responses and autoimmune diseases, was increased in the CIA+ODE group (2.5-fold) compared to Sham (Figure 8,-B).

The monocyte population ($CD11c^{-}CD11b^{+}$) was unique because all the upregulated genes including *Oasl1* (15 and 4.6-fold), *Oas1a* (15.6 and 15.3-fold), *Oas2* (11.7 and 12.4-fold), *Ifi44* (11.0 and 9.5-fold), *Ifi44l* (11.1 and 11.1-fold), *Siglec1* (11.1 and 6.1-fold), *Gbp2* (2.9 and 5.3-fold), *Gbp5* (3.8 and 4.3-fold), *Stat1* (3.3 and 3.8-fold), and *Isg15* (4.1 and 3.7-fold) were increased in both CIA and CIA+ODE groups respectively (Figure 9A-B). Moreover, these genes are mostly associated with autoimmunity or immunosuppression (27, 52). The ODE group exhibited higher transcript levels of *Ccl8* (7.5-fold), *Pdpn* (6.4-fold), *Fcrls* (4.9-fold) and *Src* (4.7-fold), consistent with the other sorted neutrophil and monocytes/macrophages populations. While *Cfb* expression was increased in all 3 treatment groups, *Dnmt3a* was upregulated (2.3 and 3.4-fold) in ODE and CIA+ODE groups, respectively (Figure 9, A-B), but not in CIA.

401 Finally, gMDSCs were identified as Ly6C^{+}Ly6G^{high}CD11b^{high}SSC^{high} (S2 Figure) (98, 99)
402 on posthoc gating of sorted neutrophil populations resulting in non-significant variations across
403 the treatment groups (Figure 10A). In contrast, mMDSC defined as Ly6G^{-} CD11b^{+} Ly6C^{high}
404 SSC^{low} cells (S2 Figure) (98, 99)were increased with CIA but decreased with ODE and CIA+ODE
405 (Figure 10B).
406

407 # Discussion

408 In this study, scRNA-seq analysis was applied to whole lung immune cells from a mouse
409 model of RA-associated inflammatory lung disease with key findings confirmed in sorted lung cell
410 populations and NanoString analysis. Building upon the preclinical model of RA-associated
411 inflammatory lung disease (11), we report a number of key findings in this study including: (a)
412 identification of 3 unique neutrophil populations including inflammatory, transient and
413 immunosuppressive/autoreactive granulocytes among experimental groups, (b) heterogeneity
414 among 5 macrophage populations including metabolically active, proliferative, differentiating,
415 recruited, and residential with classical (M1) and alternatively (M2)-activated genes, (c)
416 identification of 2 stages of T-lymphocytes (differentiating and effector), a B-cell population and
417 a NK cell cluster, (d) variability in the distribution of cellular clusters among the treatment groups
418 representing RA and RA-associated lung disease (CIA and CIA+ODE groups, respectively), (e)
419 identification of gMDSC and mMDSC populations based on cell surface markers, and (f)
420 identification of unique genes (interferon-related/autoimmune and complement cascade) that are
421 found in a mouse model of RA-associated inflammatory lung disease.

422 Occupational exposures from farming, construction, mechanics, medical and military waste
423 have been associated with increased risk of development of RA and/or RA-associated lung disease

(100-104). However, precise mechanism(s) of the development of RA-associated lung disease with occupational and/or environmental inflammatory exposures is not known. Working towards identifying these mechanisms, previous studies demonstrated that repeated exposure to microbial-enriched ODE and particularly ODE+CIA increases citrullination and malondialdehyde-acetaldehyde (MAA)-adduction of lung proteins with a corresponding increase in circulating autoantibody concentrations, periarticular bone damage, and increased deposition of extracellular matrix proteins with a reduction in classical airway inflammatory markers (11, 105). These findings suggested a transition of inflammatory lung disease towards a pro-fibrotic phenotype. Leveraging this co-exposure mouse model with CIA and ODE, several immune cell populations exhibiting unique gene expression signatures that were differentially distributed across treatment groups were demonstrated that suggest potential roles in the pathogenesis of RA, inflammatory lung disease, and inflammatory lung disease specific to RA.

Neutrophils have been classically related to inflammation and host response to pathogens (106). Knowledge of their role in inflammation and homeostasis continues to evolve as various subsets of neutrophils have been identified and proposed based upon steady state, inflammatory, or anti-inflammatory programming (107). Many intermediate phenotypes have also been defined, further complicating classifications and the proposed roles in both disease and homeostasis (108). The 3 different neutrophil populations currently identified aptly signify an inflammatory (in ODE), anti-inflammatory (or autoreactive) (in CIA and CIA+ODE) and homeostatic (transient) (in Sham). Further studies are needed to delineate precisely how these sub-populations program the lung immune response towards inflammatory and pro-fibrotic disease states.

MDSCs have been implicated in RA (109) as well as ILD (110). However, their relationship to the RA-associated lung disease is not well-established. MDSCs are transient populations

representing myeloid cells at various stages of differentiation that suppress immunity and are subdivided into granulocytic (g) or monocytic (m) origin (111-113). MDSCs are identified by their high expression of *Nox2*, calprotectin (*S100a8*/*S100a9*), *Mmp8*, *Mmp9*, *Cd33*, and multiple interferon-inducible genes such as *Ifit3*, *Ifit1*, *Oas2*, *Zbp1*, *Ifi44*, *Ifi44l* and *Oas1a* (114, 115). By scRNA-seq analysis, resolution of gMDSC was high with population segregation in cluster 3, which was driven by systemic arthritis induction (i.e. CIA and CIA+ODE groups). This finding was further strengthened by the RNA analysis of the sorted $Ly6G^{+}$ $Ly6C^{+}$ neutrophil population of corresponding treatment groups. Posthoc analysis confirmed that the sorted group contained gMDSCs with $Ly6G^{+}$ $Ly6C^{+}$ $CD11b^{high}$ SSC^{high} gating (98, 99), but there was no difference across treatment groups. Unsupervised clustering of immune cells did not segregate mMDSCs. However, gene expression of sorted monocyte-macrophage populations based on CD11b and CD11c expression suggested the presence of mMDSC-like properties based upon the immunosuppressive genes that were elevated in CIA and CIA+ODE groups. Using a classical gating strategy ($Ly6G^{-}$ $CD11b^{+}$ $Ly6C^{high}$ SSC^{low}) for mMDSCs (99), mMDSCs were identified with FACS and found to be decreased in combination (CIA+ODE) exposure group. These findings are consistent with a recent report that showed that the expansion of MDSCs following tofacitinib treatment is inversely related to the progression of ILD in the SKG mouse model of RA-ILD (116). These collective findings would suggest a potential protective role for lung MDSCs (particularly mMDSCs) in the development RA-related lung disease, and future studies are warranted to understand their role in disease manifestations to potentially develop novel targets for therapeutic interventions.

Macrophages are one of the most versatile immune cells with immense population heterogeneity and diverse functions (117, 118). Macrophages are increasingly appreciated for their role in fibrosis, wound repair and resolution (42, 63, 119). In this current study, the metabolically

active airspace macrophages, resident, recruited and differentiating macrophages (clusters 1, 11, 5 and 2, respectively) contribute to inflammation and resolution, while the proliferative airspace macrophages (cluster 14) signify self-renewing properties to maintain a steady population in the lungs. These studies potentially open avenues for hypothesis generation based on various non-traditional genes (interferon-related/autoimmune and complement cascade) expressed in the macrophage subsets that have not been previously investigated in health and disease. The unique distribution of various macrophage clusters among the treatment groups, particularly clusters 1b, 1c, 5 and 11 in ODE group, and clusters 1a, 2a and 12b (inflammatory monocytes) in CIA and CIA+ODE groups signify their importance in disease transition from RA to RA-associated lung disease.

Subtle differences among lymphocyte populations (clusters 6, 7, 9 and 13) support earlier work demonstrating that B lymphocytes are skewed towards an autoreactive response following airborne biohazard exposure (105). B lymphocytes have been recognized as one of the major drivers of autoimmunity (120) and are the target of highly effective RA therapies such as rituximab (121). Colocalization of MAA with autoreactive B lymphocytes in lung tissues of RA-ILD patients (122) further signifies their potential role in the pathogenesis of RA-ILD. While NK cells are considered a bridge between innate and adaptive immune responses (123), targeting cluster 9b could be of interest. Similarly, autoreactive T lymphocytes (perhaps cluster 6b) and cellular phenotypes supporting fibroproliferation with increase in activated fibroblasts with extracellular matrix deposition could be of particular interest in RA-ILD.

In addition to confirming the upregulation of several interferon-induced genes implicated in autoimmunity, complement cascade genes such as *C1ra*, *C1qa*, *C1qb*, *C2*, and *Cfb* representing classical and alternative pathways (124) were identified. *C1s1* was highlighted among the

493 complement cascade genes due to its high expression, and was invariably upregulated in the
494 CIA+ODE group in all 4 cell-sorted neutrophil and monocyte-macrophage populations. *C1* acts as
495 a sensor for self and non-self-recognition and thus plays a major role in self-tolerance (125).
496 Complement cascade genes are recognized in RA (126) and ILD (127-129), but remain overlooked
497 as therapeutic targets (130). Holers *et. al.* (126) suggested that RA-ILD has a complement
498 connection, but to our knowledge, this is among the first reports to experimentally identify *C1s1*
499 or complement cascade genes in a RA-inflammatory lung disease model.

500 In conclusion, application of scRNA-seq to an animal model combining systemic arthritis
501 induction and environmental inhalant-induced lung inflammation (i.e. RA-associated lung disease)
502 identified unique populations of lung immune cell clusters differentially ascribed to individual
503 treatment conditions. Neutrophil subpopulations and heterogeneous macrophage-monocyte
504 populations were identified in addition to unique genes (interferon-related and complement
505 cascade) that could be contributing to the pathogenesis of RA-associated lung disease.
506 Additionally, this information might inform potential candidates that could be exploited in future
507 investigations examining targeted interventions and the identification of informative disease
508 biomarkers.

509

510 # Acknowledgements

511 Study supported by grants from the National Institute of Environmental Health Sciences
512 (R01ES019325 to JAP; www.niehs.nih.gov), National Institute for Occupational Safety and
513 Health (U54OH010162 to JAP and TAW; www.cdc.gov/niosh/index.htm). TAW is the recipient
514 of a Research Career Scientist Award (IK6 BX003781; www.va.gov) from the Department of
515 Veterans Affairs. TRM is supported by VA (CX000896 and BX004600; www.va.gov) and grants

516 from the National Institute of General Medical Sciences (U54GM115458; www.nigms.nih.gov)
517 and the National Institute on Alcohol Abuse and Alcoholism (R25AA020818;
518 www.niaaa.nih.gov). BRE is supported by grants from the National Institute of General Medical
519 Sciences (U54GM115458; www.nigms.nih.gov) and the Rheumatology Research Foundation
520 (www.rheumresearch.org). Study also supported by the Fred & Pamela Buffett Cancer Center
521 Shared Resource, supported by the National Cancer Institute under award number P30CA036727.
522 The University of Nebraska DNA Sequencing Core and Bioinformatics Core receive partial
523 support from the National Institute for General Medical Science (NIGMS) NE-INBRE (Nebraska
524 Research Network in Functional Genomics) (P20GM103427; www.nigms.nih.gov) and COBRE
525 (1P30GM110768; www.nigms.nih.gov). This publication's contents are the sole responsibility of
526 the authors. The funders had no role in study design, data collection and analysis, decision to
527 publish, or preparation of the manuscript.

528 We thank Victoria B. Smith, Samantha D. Wall, Craig L. Semerad in the Flow Cytometry
529 Research Facility at UNMC for technical support for flow cytometry studies. We thank Jennifer
530 L. Bushing in the Sequencing Core at UNMC for assistance with NanoString studies. We also
531 thank Lisa R. Chudomelka for article preparation assistance and submission.

References

1. Aubart F, Crestani B, Nicaise-Roland P, Tubach F, Bollet C, Dawidowicz K, et al. High levels of anti-cyclic citrullinated peptide autoantibodies are associated with co-occurrence of pulmonary diseases with rheumatoid arthritis. J Rheumatol. 2011;38(6):979-82.

2. Shaw M, Collins BF, Ho LA, Raghu G. Rheumatoid arthritis-associated lung disease. Eur Respir Rev. 2015;24(135):1-16.

3. Friedlander HM, Ford JA, Zaccardelli A, Terrio AV, Cho MH, Sparks JA. Obstructive lung diseases and risk of rheumatoid arthritis. Expert Rev Clin Immunol. 2020;16(1):37-50.

4. Salaffi F, Carotti M, Di Carlo M, Tardella M, Giovagnoni A. High-resolution computed tomography of the lung in patients with rheumatoid arthritis: Prevalence of interstitial lung disease involvement and determinants of abnormalities. Medicine (Baltimore). 2019;98(38):e17088.

5. Raimundo K, Solomon JJ, Olson AL, Kong AM, Cole AL, Fischer A, et al. Rheumatoid Arthritis-Interstitial Lung Disease in the United States: Prevalence, Incidence, and Healthcare Costs and Mortality. J Rheumatol. 2019;46(4):360-9.

6. Janssen KM, de Smit MJ, Brouwer E, de Kok FA, Kraan J, Altenburg J, et al. Rheumatoid arthritis-associated autoantibodies in non-rheumatoid arthritis patients with mucosal inflammation: a case-control study. Arthritis Res Ther. 2015;17:174.

7. Perry E, Eggleton P, De Soyza A, Hutchinson D, Kelly C. Increased disease activity, severity and autoantibody positivity in rheumatoid arthritis patients with co-existent bronchiectasis. Int J Rheum Dis. 2017;20(12):2003-11.

553 8. Cassone G, Manfredi A, Vacchi C, Luppi F, Coppi F, Salvarani C, et al. Treatment of
554 Rheumatoid Arthritis-Associated Interstitial Lung Disease: Lights and Shadows. J Clin Med.
555 2020;9(4).
556 9. Wang D, Zhang J, Lau J, Wang S, Taneja V, Matteson EL, et al. Mechanisms of lung
557 disease development in rheumatoid arthritis. Nat Rev Rheumatol. 2019;15(10):581-96.
558 10. Anderson R, Meyer PW, Ally MM, Tikly M. Smoking and Air Pollution as Pro-
559 Inflammatory Triggers for the Development of Rheumatoid Arthritis. Nicotine Tob Res.
560 2016;18(7):1556-65.
561 11. Poole JA, Thiele GM, Janike K, Nelson AJ, Duryee MJ, Rentfro K, et al. Combined
562 Collagen-Induced Arthritis and Organic Dust-Induced Airway Inflammation to Model
563 Inflammatory Lung Disease in Rheumatoid Arthritis. J Bone Miner Res. 2019;34(9):1733-43.
564 12. Poole JA, Wyatt TA, Oldenburg PJ, Elliott MK, West WW, Sisson JH, et al. Intranasal
565 organic dust exposure-induced airway adaptation response marked by persistent lung
566 inflammation and pathology in mice. Am J Physiol Lung Cell Mol Physiol. 2009;296(6):L1085-
567 95.
568 13. 10x Genomics. What is Loupe Browser? 2020 [Available from:
569 https://support.10xgenomics.com/single-cell-gene-expression/software/visualization/latest/what-
570 is-loupe-cell-browser.
571 14. Genomics x. Cell Ranger R Kit Tutorial: Secondary Analysis on 10x Genomics Single
572 Cell 3' RNA-seq PBMC Data 2017 [updated 18 July. Available from:
573 http://cf.10xgenomics.com/supp/cell-exp/cellrangerrkit-PBMC-vignette-knitr-2.0.0.pdf.
574 15. Gu Z, Eils R, Schlesner M. Complex heatmaps reveal patterns and correlations in
575 multidimensional genomic data. Bioinformatics. 2016;32(18):2847-9.

576 16. Hintze JL, Nelson, R. D. Violin Plots: A Box Plot-Density Trace Synergism. The
577 American Statistician. 1998;52(2):181-4.
578 17. Basheer F, Rasighaemi P, Liongue C, Ward AC. Zebrafish Granulocyte Colony-
579 Stimulating Factor Receptor Maintains Neutrophil Number and Function throughout the Life
580 Span. Infect Immun. 2019;87(2):e00793-18.
581 18. Hartl D, Krauss-Etschmann S, Koller B, Hordijk PL, Kuijpers TW, Hoffmann F, et al.
582 Infiltrated neutrophils acquire novel chemokine receptor expression and chemokine
583 responsiveness in chronic inflammatory lung diseases. J Immunol. 2008;181(11):8053-67.
584 19. Sokol CL, Luster AD. The chemokine system in innate immunity. Cold Spring Harb
585 Perspect Biol. 2015;7(5):a016303.
586 20. Tang BM, Shojaei M, Teoh S, Meyers A, Ho J, Ball TB, et al. Neutrophils-related host
587 factors associated with severe disease and fatality in patients with influenza infection. Nat
588 Commun. 2019;10(1):3422.
589 21. El Amri M, Fitzgerald U, Schlosser G. MARCKS and MARCKS-like proteins in
590 development and regeneration. J Biomed Sci. 2018;25(1):43.
591 22. Sheats MK, Pescosolido KC, Hefner EM, Sung EJ, Adler KB, Jones SL. Myristoylated
592 Alanine Rich C Kinase Substrate (MARCKS) is essential to beta2-integrin dependent responses
593 of equine neutrophils. Vet Immunol Immunopathol. 2014;160(3-4):167-76.
594 23. Sinha P, Okoro C, Foell D, Freeze HH, Ostrand-Rosenberg S, Srikrishna G.
595 Proinflammatory S100 proteins regulate the accumulation of myeloid-derived suppressor cells. J
596 Immunol. 2008;181(7):4666-75.

24. Yang J, Anholts J, Kolbe U, Stegehuis-Kamp JA, Claas FHJ, Eikmans M. Calcium-Binding Proteins S100A8 and S100A9: Investigation of Their Immune Regulatory Effect in Myeloid Cells. Int J Mol Sci. 2018;19(7):1833.

25. Uhel F, Azzaoui I, Gregoire M, Pangault C, Dulong J, Tadie JM, et al. Early Expansion of Circulating Granulocytic Myeloid-derived Suppressor Cells Predicts Development of Nosocomial Infections in Patients with Sepsis. Am J Respir Crit Care Med. 2017;196(3):315-27.

26. Taleb K, Auffray C, Villefroy P, Pereira A, Hosmalin A, Gaudry M, et al. Chronic Type I IFN Is Sufficient To Promote Immunosuppression through Accumulation of Myeloid-Derived Suppressor Cells. J Immunol. 2017;198(3):1156-63.

27. van der Pouw Kraan TC, Wijbrandts CA, van Baarsen LG, Voskuyl AE, Rustenburg F, Baggen JM, et al. Rheumatoid arthritis subtypes identified by genomic profiling of peripheral blood cells: assignment of a type I interferon signature in a subpopulation of patients. Ann Rheum Dis. 2007;66(8):1008-14.

28. Hassan M, Raslan HM, Eldin HG, Mahmoud E, Elwajed HAA. CD33(+) HLA-DR(-) Myeloid-Derived Suppressor Cells Are Increased in Frequency in the Peripheral Blood of Type1 Diabetes Patients with Predominance of CD14(+) Subset. Open Access Maced J Med Sci. 2018;6(2):303-9.

29. Okano S, Abu-Elmagd K, Kish DD, Keslar K, Baldwin WM, 3rd, Fairchild RL, et al. Myeloid-derived suppressor cells increase and inhibit donor-reactive T cell responses to graft intestinal epithelium in intestinal transplant patients. Am J Transplant. 2018;18(10):2544-58.

30. Martin P, Palmer G, Vigne S, Lamacchia C, Rodriguez E, Talabot-Ayer D, et al. Mouse neutrophils express the decoy type 2 interleukin-1 receptor (IL-1R2) constitutively and in acute inflammatory conditions. J Leukoc Biol. 2013;94(4):791-802.

620 31. Shimizu K, Nakajima A, Sudo K, Liu Y, Mizoroki A, Ikarashi T, et al. IL-1 receptor type
621 2 suppresses collagen-induced arthritis by inhibiting IL-1 signal on macrophages. J Immunol.
622 2015;194(7):3156-68.
623 32. Abboud S, Haile DJ. A novel mammalian iron-regulated protein involved in intracellular
624 iron metabolism. J Biol Chem. 2000;275(26):19906-12.
625 33. Eash KJ, Greenbaum AM, Gopalan PK, Link DC. CXCR2 and CXCR4 antagonistically
626 regulate neutrophil trafficking from murine bone marrow. J Clin Invest. 2010;120(7):2423-31.
627 34. Manley HR, Keightley MC, Lieschke GJ. The Neutrophil Nucleus: An Important
628 Influence on Neutrophil Migration and Function. Front Immunol. 2018;9:2867.
629 35. Shin JW, Spinler KR, Swift J, Chasis JA, Mohandas N, Discher DE. Lamins regulate cell
630 trafficking and lineage maturation of adult human hematopoietic cells. Proc Natl Acad Sci U S
631 A. 2013;110(47):18892-7.
632 36. Ouzounova M, Lee E, Piranlioglu R, El Andaloussi A, Kolhe R, Demirci MF, et al.
633 Monocytic and granulocytic myeloid derived suppressor cells differentially regulate
634 spatiotemporal tumour plasticity during metastatic cascade. Nat Commun. 2017;8:14979.
635 37. Goulart MR, Hlavaty SI, Chang YM, Polton G, Stell A, Perry J, et al. Phenotypic and
636 transcriptomic characterization of canine myeloid-derived suppressor cells. Sci Rep.
637 2019;9(1):3574.
638 38. Cormier SA, Yuan S, Crosby JR, Protheroe CA, Dimina DM, Hines EM, et al. T(H)2-
639 mediated pulmonary inflammation leads to the differential expression of ribonuclease genes by
640 alveolar macrophages. Am J Respir Cell Mol Biol. 2002;27(6):678-87.

641 39. Bosurgi L, Cao YG, Cabeza-Cabrerizo M, Tucci A, Hughes LD, Kong Y, et al.
642 Macrophage function in tissue repair and remodeling requires IL-4 or IL-13 with apoptotic cells.
643 Science. 2017;356(6342):1072-6.
644 40. Long EK, Hellberg K, Foncea R, Hertzel AV, Suttles J, Bernlohr DA. Fatty acids induce
645 leukotriene C4 synthesis in macrophages in a fatty acid binding protein-dependent manner.
646 Biochim Biophys Acta. 2013;1831(7):1199-207.
647 41. Schachtrup C, Scholzen TE, Grau V, Luger TA, Sorg C, Spener F, et al. L-FABP is
648 exclusively expressed in alveolar macrophages within the myeloid lineage: evidence for a
649 PPARalpha-independent expression. Int J Biochem Cell Biol. 2004;36(10):2042-53.
650 42. Gibbings SL, Thomas SM, Atif SM, McCubbrey AL, Desch AN, Danhorn T, et al. Three
651 Unique Interstitial Macrophages in the Murine Lung at Steady State. Am J Respir Cell Mol Biol.
652 2017;57(1):66-76.
653 43. Zuo Y, d'Aigle J, Chauhan A, Frost JA. Genetic deletion of the Rho GEF Net1 impairs
654 mouse macrophage motility and actin cytoskeletal organization. Small GTPases. 2017:1-8.
655 44. Wojcik AJ, Skaflen MD, Srinivasan S, Hedrick CC. A critical role for ABCG1 in
656 macrophage inflammation and lung homeostasis. J Immunol. 2008;180(6):4273-82.
657 45. Shayman JA, Tesmer JJG. Lysosomal phospholipase A2. Biochim Biophys Acta Mol
658 Cell Biol Lipids. 2019;1864(6):932-40.
659 46. Abe A, Hiraoka M, Wild S, Wilcoxen SE, Paine R, 3rd, Shayman JA. Lysosomal
660 phospholipase A2 is selectively expressed in alveolar macrophages. J Biol Chem.
661 2004;279(41):42605-11.

662 47. Zhou Y, Do DC, Ishmael FT, Squadrito ML, Tang HM, Tang HL, et al. Mannose
663 receptor modulates macrophage polarization and allergic inflammation through miR-511-3p. J
664 Allergy Clin Immunol. 2018;141(1):350-64 e8.
665 48. Li D, Duan M, Feng Y, Geng L, Li X, Zhang W. MiR-146a modulates macrophage
666 polarization in systemic juvenile idiopathic arthritis by targeting INHBA. Mol Immunol.
667 2016;77:205-12.
668 49. Morse C, Tabib T, Sembrat J, Buschur KL, Bittar HT, Valenzi E, et al. Proliferating
669 SPP1/MERTK-expressing macrophages in idiopathic pulmonary fibrosis. Eur Respir J.
670 2019;54(2):1802441.
671 50. Naito Y, Takagi T, Higashimura Y. Heme oxygenase-1 and anti-inflammatory M2
672 macrophages. Arch Biochem Biophys. 2014;564:83-8.
673 51. Patsalos A, Tzerpos P, Halasz L, Nagy G, Pap A, Giannakis N, et al. The BACH1-
674 HMOX1 Regulatory Axis Is Indispensable for Proper Macrophage Subtype Specification and
675 Skeletal Muscle Regeneration. J Immunol. 2019;203(6):1532-47.
676 52. Wammers M, Schupp AK, Bode JG, Ehlting C, Wolf S, Deenen R, et al. Reprogramming
677 of pro-inflammatory human macrophages to an anti-inflammatory phenotype by bile acids. Sci
678 Rep. 2018;8(1):255.
679 53. Kusuyama J, Komorizono A, Bandow K, Ohnishi T, Matsuguchi T. CXCL3 positively
680 regulates adipogenic differentiation. J Lipid Res. 2016;57(10):1806-20.
681 54. Szondy Z, Sarang Z, Molnar P, Nemeth T, Piacentini M, Mastroberardino PG, et al.
682 Transglutaminase 2-/- mice reveal a phagocytosis-associated crosstalk between macrophages and
683 apoptotic cells. Proc Natl Acad Sci U S A. 2003;100(13):7812-7.

684 55. Toth B, Garabuczi E, Sarang Z, Vereb G, Vamosi G, Aeschlimann D, et al.
685 Transglutaminase 2 is needed for the formation of an efficient phagocyte portal in macrophages
686 engulfing apoptotic cells. J Immunol. 2009;182(4):2084-92.
687 56. Yu X, Buttgereit A, Lelios I, Utz SG, Cansever D, Becher B, et al. The Cytokine TGF-
688 beta Promotes the Development and Homeostasis of Alveolar Macrophages. Immunity.
689 2017;47(5):903-12 e4.
690 57. Lavin Y, Winter D, Blecher-Gonen R, David E, Keren-Shaul H, Merad M, et al. Tissue-
691 resident macrophage enhancer landscapes are shaped by the local microenvironment. Cell.
692 2014;159(6):1312-26.
693 58. Baitsch D, Bock HH, Engel T, Telgmann R, Muller-Tidow C, Varga G, et al.
694 Apolipoprotein E induces antiinflammatory phenotype in macrophages. Arterioscler Thromb
695 Vasc Biol. 2011;31(5):1160-8.
696 59. Zmijewski JW, Banerjee S, Abraham E. S-glutathionylation of the Rpn2 regulatory
697 subunit inhibits 26 S proteasomal function. J Biol Chem. 2009;284(33):22213-21.
698 60. Chen G, Tan CS, Teh BK, Lu J. Molecular mechanisms for synchronized transcription of
699 three complement C1q subunit genes in dendritic cells and macrophages. J Biol Chem.
700 2011;286(40):34941-50.
701 61. Verneret M, Tacnet-Delorme P, Osman R, Awad R, Grichine A, Kleman JP, et al.
702 Relative contribution of c1q and apoptotic cell-surface calreticulin to macrophage phagocytosis.
703 J Innate Immun. 2014;6(4):426-34.
704 62. Osman R, Tacnet-Delorme P, Kleman JP, Millet A, Frachet P. Calreticulin Release at an
705 Early Stage of Death Modulates the Clearance by Macrophages of Apoptotic Cells. Front
706 Immunol. 2017;8:1034.

63. Mould KJ, Jackson ND, Henson PM, Seibold M, Janssen WJ. Single cell RNA sequencing identifies unique inflammatory airspace macrophage subsets. JCI Insight. 2019;4(5):e126556.

64. Nuncia-Cantarero M, Martinez-Canales S, Andres-Pretel F, Santpere G, Ocana A, Galan-Moya EM. Functional transcriptomic annotation and protein-protein interaction network analysis identify NEK2, BIRC5, and TOP2A as potential targets in obese patients with luminal A breast cancer. Breast Cancer Res Treat. 2018;168(3):613-23.

65. Tang-Huau TL, Gueguen P, Goudot C, Durand M, Bohec M, Baulande S, et al. Human in vivo-generated monocyte-derived dendritic cells and macrophages cross-present antigens through a vacuolar pathway. Nat Commun. 2018;9(1):2570.

66. Porrello A, Leslie PL, Harrison EB, Gorentla BK, Kattula S, Ghosh SK, et al. Factor XIIIA-expressing inflammatory monocytes promote lung squamous cancer through fibrin cross-linking. Nat Commun. 2018;9(1):1988.

67. Briseno CG, Haldar M, Kretzer NM, Wu X, Theisen DJ, Kc W, et al. Distinct Transcriptional Programs Control Cross-Priming in Classical and Monocyte-Derived Dendritic Cells. Cell Rep. 2016;15(11):2462-74.

68. Sanyal R, Polyak MJ, Zuccolo J, Puri M, Deng L, Roberts L, et al. MS4A4A: a novel cell surface marker for M2 macrophages and plasma cells. Immunol Cell Biol. 2017;95(7):611-9.

69. Hey YY, O'Neill TJ, O'Neill HC. A novel myeloid cell in murine spleen defined through gene profiling. J Cell Mol Med. 2019;23(8):5128-43.

70. Segawa S, Kondo Y, Nakai Y, Iizuka A, Kaneko S, Yokosawa M, et al. Placenta Specific 8 Suppresses IL-18 Production through Regulation of Autophagy and Is Associated with Adult Still Disease. J Immunol. 2018;201(12):3534-45.

730 71. Kuroda N, Masuya M, Tawara I, Tsuboi J, Yoneda M, Nishikawa K, et al. Infiltrating
731 CCR2(+) monocytes and their progenies, fibrocytes, contribute to colon fibrosis by inhibiting
732 collagen degradation through the production of TIMP-1. Sci Rep. 2019;9(1):8568.
733 72. Lim JK, Obara CJ, Rivollier A, Pletnev AG, Kelsall BL, Murphy PM. Chemokine
734 receptor Ccr2 is critical for monocyte accumulation and survival in West Nile virus encephalitis.
735 J Immunol. 2011;186(1):471-8.
736 73. Coates BM, Staricha KL, Koch CM, Cheng Y, Shumaker DK, Budinger GRS, et al.
737 Inflammatory Monocytes Drive Influenza A Virus-Mediated Lung Injury in Juvenile Mice. J
738 Immunol. 2018;200(7):2391-404.
739 74. Bajpai G, Bredemeyer A, Li W, Zaitsev K, Koenig AL, Lokshina I, et al. Tissue Resident
740 CCR2- and CCR2+ Cardiac Macrophages Differentially Orchestrate Monocyte Recruitment and
741 Fate Specification Following Myocardial Injury. Circ Res. 2019;124(2):263-78.
742 75. Blasius AL, Cella M, Maldonado J, Takai T, Colonna M. Siglec-H is an IPC-specific
743 receptor that modulates type I IFN secretion through DAP12. Blood. 2006;107(6):2474-6.
744 76. Zhang J, Raper A, Sugita N, Hingorani R, Salio M, Palmowski MJ, et al.
745 Characterization of Siglec-H as a novel endocytic receptor expressed on murine plasmacytoid
746 dendritic cell precursors. Blood. 2006;107(9):3600-8.
747 77. Grajkowska LT, Ceribelli M, Lau CM, Warren ME, Tiniakou I, Nakandakari Higa S, et
748 al. Isoform-Specific Expression and Feedback Regulation of E Protein TCF4 Control Dendritic
749 Cell Lineage Specification. Immunity. 2017;46(1):65-77.
750 78. Gueguen C, Bouley J, Moussu H, Luce S, Duchateau M, Chamot-Rooke J, et al. Changes
751 in markers associated with dendritic cells driving the differentiation of either TH2 cells or

752 regulatory T cells correlate with clinical benefit during allergen immunotherapy. J Allergy Clin
753 Immunol. 2016;137(2):545-58.
754 79. Zimmermann HW, Bruns T, Weston CJ, Curbishley SM, Liaskou E, Li KK, et al.
755 Bidirectional transendothelial migration of monocytes across hepatic sinusoidal endothelium
756 shapes monocyte differentiation and regulates the balance between immunity and tolerance in
757 liver. Hepatology. 2016;63(1):233-46.
758 80. Cao W, Bover L, Cho M, Wen X, Hanabuchi S, Bao M, et al. Regulation of TLR7/9
759 responses in plasmacytoid dendritic cells by BST2 and ILT7 receptor interaction. J Exp Med.
760 2009;206(7):1603-14.
761 81. Bego MG, Miguet N, Laliberte A, Aschman N, Gerard F, Merakos AA, et al. Activation
762 of the ILT7 receptor and plasmacytoid dendritic cell responses are governed by structurally-
763 distinct BST2 determinants. J Biol Chem. 2019;294(27):10503-18.
764 82. Xing S, Li F, Zeng Z, Zhao Y, Yu S, Shan Q, et al. Tcf1 and Lef1 transcription factors
765 establish CD8(+) T cell identity through intrinsic HDAC activity. Nat Immunol. 2016;17(6):695-
766 703.
767 83. Willinger T, Freeman T, Herbert M, Hasegawa H, McMichael AJ, Callan MF. Human
768 naive CD8 T cells down-regulate expression of the WNT pathway transcription factors lymphoid
769 enhancer binding factor 1 and transcription factor 7 (T cell factor-1) following antigen encounter
770 in vitro and in vivo. J Immunol. 2006;176(3):1439-46.
771 84. Maier E, Hebenstreit D, Posselt G, Hammerl P, Duschl A, Horejs-Hoeck J. Inhibition of
772 suppressive T cell factor 1 (TCF-1) isoforms in naive CD4+ T cells is mediated by IL-4/STAT6
773 signaling. J Biol Chem. 2011;286(2):919-28.

774 85. Doucey MA, Goffin L, Naeher D, Michielin O, Baumgartner P, Guillaume P, et al. CD3
775 delta establishes a functional link between the T cell receptor and CD8. J Biol Chem.
776 2003;278(5):3257-64.
777 86. Borroto A, Lama J, Niedergang F, Dautry-Varsat A, Alarcon B, Alcover A. The CD3
778 epsilon subunit of the TCR contains endocytosis signals. J Immunol. 1999;163(1):25-31.
779 87. Nechanitzky R, Akbas D, Scherer S, Gyory I, Hoyler T, Ramamoorthy S, et al.
780 Transcription factor EBF1 is essential for the maintenance of B cell identity and prevention of
781 alternative fates in committed cells. Nat Immunol. 2013;14(8):867-75.
782 88. Luisiri P, Lee YJ, Eisfelder BJ, Clark MR. Cooperativity and segregation of function
783 within the Ig-alpha/beta heterodimer of the B cell antigen receptor complex. J Biol Chem.
784 1996;271(9):5158-63.
785 89. Tedder TF, Streuli M, Schlossman SF, Saito H. Isolation and structure of a cDNA
786 encoding the B1 (CD20) cell-surface antigen of human B lymphocytes. Proc Natl Acad Sci U S
787 A. 1988;85(1):208-12.
788 90. McHeyzer-Williams M, Okitsu S, Wang N, McHeyzer-Williams L. Molecular
789 programming of B cell memory. Nat Rev Immunol. 2011;12(1):24-34.
790 91. Sheppard S, Schuster IS, Andoniou CE, Cocita C, Adejumo T, Kung SKP, et al. The
791 Murine Natural Cytotoxic Receptor NKp46/NCR1 Controls TRAIL Protein Expression in NK
792 Cells and ILC1s. Cell Rep. 2018;22(13):3385-92.
793 92. Bottcher JP, Bonavita E, Chakravarty P, Blees H, Cabeza-Cabrerizo M, Sammicheli S, et
794 al. NK Cells Stimulate Recruitment of cDC1 into the Tumor Microenvironment Promoting
795 Cancer Immune Control. Cell. 2018;172(5):1022-37 e14.

796 93. Bade B, Boettcher HE, Lohrmann J, Hink-Schauer C, Bratke K, Jenne DE, et al.
797 Differential expression of the granzymes A, K and M and perforin in human peripheral blood
798 lymphocytes. Int Immunol. 2005;17(11):1419-28.
799 94. Pardo J, Balkow S, Anel A, Simon MM. Granzymes are essential for natural killer cell-
800 mediated and perf-facilitated tumor control. Eur J Immunol. 2002;32(10):2881-7.
801 95. Turman MA, Yabe T, McSherry C, Bach FH, Houchins JP. Characterization of a novel
802 gene (NKG7) on human chromosome 19 that is expressed in natural killer cells and T cells. Hum
803 Immunol. 1993;36(1):34-40.
804 96. Medley QG, Kedersha N, O'Brien S, Tian Q, Schlossman SF, Streuli M, et al.
805 Characterization of GMP-17, a granule membrane protein that moves to the plasma membrane of
806 natural killer cells following target cell recognition. Proc Natl Acad Sci U S A. 1996;93(2):685-
807 9.
808 97. Poole JA, Gleason AM, Bauer C, West WW, Alexis N, van Rooijen N, et al.
809 CD11c(+)/CD11b(+) cells are critical for organic dust-elicited murine lung inflammation. Am J
810 Respir Cell Mol Biol. 2012;47(5):652-9.
811 98. Bronte V, Brandau S, Chen SH, Colombo MP, Frey AB, Greten TF, et al.
812 Recommendations for myeloid-derived suppressor cell nomenclature and characterization
813 standards. Nat Commun. 2016;7:12150.
814 99. Damuzzo V, Pinton L, Desantis G, Solito S, Marigo I, Bronte V, et al. Complexity and
815 challenges in defining myeloid-derived suppressor cells. Cytometry B Clin Cytom.
816 2015;88(2):77-91.
817 100. Karlson EW, Deane K. Environmental and gene-environment interactions and risk of
818 rheumatoid arthritis. Rheum Dis Clin North Am. 2012;38(2):405-26.

819 101. Murphy D, Bellis K, Hutchinson D. Vapour, gas, dust and fume occupational exposures
820 in male patients with rheumatoid arthritis resident in Cornwall (UK) and their association with
821 rheumatoid factor and anti-cyclic protein antibodies: a retrospective clinical study. BMJ Open.
822 2018;8(5):e021754.
823 102. Murphy D, Bellis K, Hutchinson D. Occupational dust and cigarette smoke exposure
824 might link rheumatoid arthritis to COPD. Lancet Respir Med. 2018;6(8):e36.
825 103. Murphy D, Hutchinson D. Is Male Rheumatoid Arthritis an Occupational Disease? A
826 Review. Open Rheumatol J. 2017;11:88-105.
827 104. Szema AM. Occupational Lung Diseases among Soldiers Deployed to Iraq and
828 Afghanistan. Occup Med Health Aff. 2013;1.
829 105. Poole JA, Mikuls TR, Duryee MJ, Warren KJ, Wyatt TA, Nelson AJ, et al. A role for B
830 cells in organic dust induced lung inflammation. Respir Res. 2017;18(1):214.
831 106. Mortaz E, Alipoor SD, Adcock IM, Mumby S, Koenderman L. Update on Neutrophil
832 Function in Severe Inflammation. Front Immunol. 2018;9:2171.
833 107. Rosales C. Neutrophil: A Cell with Many Roles in Inflammation or Several Cell Types?
834 Front Physiol. 2018;9:113.
835 108. Tsuda Y, Takahashi H, Kobayashi M, Hanafusa T, Herndon DN, Suzuki F. Three
836 different neutrophil subsets exhibited in mice with different susceptibilities to infection by
837 methicillin-resistant Staphylococcus aureus. Immunity. 2004;21(2):215-26.
838 109. Zhu J, Chen S, Wu L, Wang R, Zheng S, Zhao D, et al. The Expansion of Myeloid-
839 Derived Suppressor Cells Is Associated with Joint Inflammation in Rheumatic Patients with
840 Arthritis. Biomed Res Int. 2018;2018:5474828.

110. Fernandez IE, Greiffo FR, Frankenberger M, Bandres J, Heinzelmann K, Neurohr C, et al. Peripheral blood myeloid-derived suppressor cells reflect disease status in idiopathic pulmonary fibrosis. Eur Respir J. 2016;48(4):1171-83.

111. Almand B, Clark JI, Nikitina E, van Beynen J, English NR, Knight SC, et al. Increased production of immature myeloid cells in cancer patients: a mechanism of immunosuppression in cancer. J Immunol. 2001;166(1):678-89.

112. Bronte V, Serafini P, Apolloni E, Zanovello P. Tumor-induced immune dysfunctions caused by myeloid suppressor cells. J Immunother. 2001;24(6):431-46.

113. Melani C, Chiodoni C, Forni G, Colombo MP. Myeloid cell expansion elicited by the progression of spontaneous mammary carcinomas in c-erbB-2 transgenic BALB/c mice suppresses immune reactivity. Blood. 2003;102(6):2138-45.

114. Ohl K, Tenbrock K. Reactive Oxygen Species as Regulators of MDSC-Mediated Immune Suppression. Front Immunol. 2018;9:2499.

115. Groth C, Hu X, Weber R, Fleming V, Altevogt P, Utikal J, et al. Immunosuppression mediated by myeloid-derived suppressor cells (MDSCs) during tumour progression. Br J Cancer. 2019;120(1):16-25.

116. Sendo S, Saegusa J, Yamada H, Nishimura K, Morinobu A. Tofacitinib facilitates the expansion of myeloid-derived suppressor cells and ameliorates interstitial lung disease in SKG mice. Arthritis Res Ther. 2019;21(1):184.

117. Gordon S, Pluddemann A, Martinez Estrada F. Macrophage heterogeneity in tissues: phenotypic diversity and functions. Immunol Rev. 2014;262(1):36-55.

118. Kielbassa K, Vegna S, Ramirez C, Akkari L. Understanding the Origin and Diversity of Macrophages to Tailor Their Targeting in Solid Cancers. Front Immunol. 2019;10:2215.

119. Wynn TA, Vannella KM. Macrophages in Tissue Repair, Regeneration, and Fibrosis. Immunity. 2016;44(3):450-62.

120. Rawlings DJ, Metzler G, Wray-Dutra M, Jackson SW. Altered B cell signalling in autoimmunity. Nat Rev Immunol. 2017;17(7):421-36.

121. Hofmann K, Clauder AK, Manz RA. Targeting B Cells and Plasma Cells in Autoimmune Diseases. Front Immunol. 2018;9:835.

122. England BR, Duryee MJ, Roul P, Mahajan TD, Singh N, Poole JA, et al. Malondialdehyde-Acetaldehyde Adducts and Antibody Responses in Rheumatoid Arthritis-Associated Interstitial Lung Disease. Arthritis Rheumatol. 2019;71(9):1483-93.

123. Gianchecchi E, Delfino DV, Fierabracci A. NK cells in autoimmune diseases: Linking innate and adaptive immune responses. Autoimmun Rev. 2018;17(2):142-54.

124. Trouw LA, Pickering MC, Blom AM. The complement system as a potential therapeutic target in rheumatic disease. Nat Rev Rheumatol. 2017;13(9):538-47.

125. Botto M, Walport MJ. C1q, autoimmunity and apoptosis. Immunobiology. 2002;205(4-5):395-406.

126. Holers VM, Banda NK. Complement in the Initiation and Evolution of Rheumatoid Arthritis. Front Immunol. 2018;9:1057.

127. Gu H, Mickler EA, Cummings OW, Sandusky GE, Weber DJ, Gracon A, et al. Crosstalk between TGF-beta1 and complement activation augments epithelial injury in pulmonary fibrosis. FASEB J. 2014;28(10):4223-34.

128. Gu H, Fisher AJ, Mickler EA, Duerson F, 3rd, Cummings OW, Peters-Golden M, et al. Contribution of the anaphylatoxin receptors, C3aR and C5aR, to the pathogenesis of pulmonary fibrosis. FASEB J. 2016;30(6):2336-50.

887 129. Okamoto T, Mathai SK, Hennessy CE, Hancock LA, Walts AD, Stefanski AL, et al. The
888 relationship between complement C3 expression and the MUC5B genotype in pulmonary
889 fibrosis. Am J Physiol Lung Cell Mol Physiol. 2018;315(1):L1-L10.
890 130. Kulkarni HS, Liszewski MK, Brody SL, Atkinson JP. The complement system in the
891 airway epithelium: An overlooked host defense mechanism and therapeutic target? J Allergy
892 Clin Immunol. 2018;141(5):1582-6 e1.
893
894

Figure legends

Figure 1: Unsupervised single-cell transcriptional profiling of lung CD45$^+$ cells identifies 14 unique clusters among Sham, CIA, ODE, and CIA+ODE treatment groups. Lung immune cells were isolated from mice treated with Sham, CIA, ODE and CIA+ODE. (**A**) T-distributed stochastic neighbor embedding (*t-SNE*) plot shows projection of unique molecular identifier (UMI) count among cell clusters. (**B**) Distribution of cells by unsupervised clustering in *t-SNE* showing lung immune cell populations. (**C**) Major lung cell types identified by signature genes including *Csf3r* (neutrophils), *Cd11c/Itgax* (macrophages), *F13a1* (monocytes), *Trbc2* (T lymphocytes), *Cd19* (B lymphocytes), *Ccl5* (NK cells), and *Siglech* (dendritic cells).

Figure 2: Distribution of aggregated gene clusters among treatment groups.
Sham, CIA, ODE and CIA+ODE treatment groups demonstrate differences in cell distribution among 14 gene clusters. Sham is represented by red, CIA by green, ODE by teal, CIA+ODE by blue. (**A**) All the treatment groups are merged with respective colors. (**B**) The four treatment groups are individually plotted with their respective colors to show cell distribution.

Figure 3: Neutrophil populations segregated by unsupervised clustering relate to cell-programming among treatment groups. (**A**) Heatmap shows the top 120/N upregulated genes for 3 distinct neutrophil clusters ranked by log2 fold-change, where N=total number of clusters. (**B**) Top 5-10 genes of the three neutrophil clusters plotted in heatmap to show differences and gene names in transcript levels. (**C**) Violin plots show expression with population distribution among inflammatory neutrophils, represented by blue (cluster 8), resident/transitional neutrophils, represented by green (cluster 4) and granulocytic myeloid-derived suppressor cells

(gMDSC)/autoreactive neutrophils, represented by red (cluster 3). The y-axis indicates normalized expression value, log2 (average UMI count + 1). (**D**) Representative gene from each neutrophil cluster showing their distribution in t-SNE.

Figure 4: Differences in transcript levels among monocyte-macrophages and dendritic cell (DC) populations. (**A**) Heatmap shows the top 120/N upregulated genes for 7 macrophages/monocytes and DC clusters ranked by log2 fold-change, where N=total number of clusters. (**B**) Heatmap showing differences among top 5 genes with gene names of the macrophages/monocytes and DC populations. (**C**) Expression levels with violin plots among airspace macrophages (red, cluster 1), differentiating/recruited macrophages (brown, cluster 2), recruited macrophages (green, cluster 5), resident/interstitial macrophages (teal, cluster 11), proliferative airspace macrophages (light blue, cluster 14), inflammatory monocytes (lavender, cluster 12), dendritic cells (pink, cluster 10). The y-axis indicates normalized expression value, log2 (average UMI count + 1). (**D**) Distribution of respective cell populations by a representative gene in t-SNE plot.

Figure 5: Four discrete lymphocyte populations suggest heterogeneity among treatment groups. (**A**) Heatmap shows the top 120/N upregulated genes for 5 distinct lymphocyte clusters ranked by log2 fold-change, where N=total number of clusters. (**B**) The top 5 genes with gene names of each lymphocyte cluster are shown in heatmap. (**C**) Violin plots show variability in transcript levels among cell populations including T lymphocytes (red, cluster 6), effector T lymphocytes (green, cluster 13), B lymphocytes (teal, cluster 7) and natural killer cells (lavender,

cluster 9). The y-axis indicates normalized expression value, log2 (average UMI count + 1). (**D**) Representative genes from each cluster show their distribution in t-SNE plot.

Figure 6: Treatment group-specific gene expression pattern demonstrated in isolated lung neutrophils. Neutrophils were sorted from lung digests as live, singlets, $CD45^+$, non-lymphocytes, $Ly6C^+$ and $Ly6G^+$. (**A**) Representative dot plots of $Ly6C^+$ $Ly6G^+$ neutrophils sorted from Sham, CIA, ODE and CIA+ODE treatment groups shown. (**B**) Heat map of fold-change of top 15 genes normalized to 20 housekeeping genes from each treatment group compared to Sham. (**C**) Bar graphs reflect the mean of normalized fold-change with standard error bars of representative genes from each treatment group Sham (red), CIA (green), ODE (teal), and CIA+ODE (blue). N=3 (3 independent experiments with 2-3 mice pooled). *P<0.05, **P<0.01, ***P<0.001, ****P<0.0001.

Figure 7: Treatment group-specific gene expression pattern demonstrated in isolated macrophages Three monocyte/macrophage populations were sorted from lung digests as live, singlets, $CD45^+$, non-lymphocytes, $Ly6C^-$ and $Ly6G^-$, and identified as separate populations with variable expression of CD11b and CD11c. RNA was isolated from these populations and subjected to NanoString nCounter analysis. (**A**) Representative dot plots of the populations sorted as: (1) macrophages ($CD11c^{high}$, $CD11b^{variable}$), (2) monocytes-macrophages ($CD11c^{intermediate}$,$CD11b^{high}$), and (3) monocytes ($CD11c^-$, $CD11b^{high}$) from each treatment of Sham, CIA, ODE, and CIA+ODE shown. (**B**) Heat map of fold-change of top 15 genes normalized to 20 housekeeping genes from each treatment group compared to Sham. (**C**) Bar graphs depict mean with standard error bars of representative genes from each treatment group Sham (red), CIA (green), ODE (teal), and

963 CIA+ODE (blue). N=3 (3 independent experiments with 2-3 mice pooled). *P<0.05, **P<0.01,
964 ***P<0.001, ****P<0.0001.
965
966 **Figure 8: Treatment group-specific gene expression pattern demonstrated is isolated**
967 **monocyte-macrophage popuation.** Monocytes-macrophages were sorted as
968 $CD11c^{intermediate}$,$CD11b^{high}$. (**A**) Heat map of fold-change of top 15 genes/treatment group (CIA,
969 ODE and CIA+ODE) normalized to 20 housekeeping genes compared to Sham. (**B**) Bar graphs of
970 mean with standard error bars of representative genes from each treatment group Sham (red), CIA
971 (green), ODE (teal), and CIA+ODE (blue). N=3 (3 independent experiments with 2-3 mice
972 pooled). ***P<0.001, ****P<0.0001.
973
974 **Figure 9: Treatment group-specific gene expression pattern. Demonstrated in isolated**
975 **monocytes.** Monocytes were sorted as $CD11c^{-}$, $CD11b^{high}$. (**A**) Heat map of fold-change of top 15
976 genes/treatment group (CIA, ODE and CIA+ODE) normalized to 20 housekeeping genes
977 compared to Sham. (**B**) Bar graphs depict mean with standard error bars of representative genes
978 from each treatment group Sham (red), CIA (green), ODE (teal), and CIA+ODE (blue). Two-way
979 ANOVA, *P<0.05, ****P<0.0001.
980
981 **Figure 10: Differences in myeloid-derived suppressor cells (MDSCs) identified in posthoc**
982 **analysis among treatment groups.** (**A**) Dot plots show differences in $CD45^{+}$ $Ly6C^{+}$ $Ly6G^{+}$
983 $CD11b^{+}$ SSC^{high} granulocytic (g) MDSCs among treatment groups. (**B**) Bar graph depicts mean
984 with standard error bars of the ratio change in gMDSCs as normalized to Sham (percentile of
985 gMDSC treatment group divided by percentile of gMDSC Sham group). (**C**) Dot plots show

differences in $CD45^{+}$ $Ly6G^{-}$ $CD11b^{+}$ $Ly6C^{+}$ SSC^{low} monocytic (m) MDSCs among treatment groups. (**D**) Bar graph depicts mean with standard error bars of the ratio change in mMDSCs as normalized to Sham (percentile of mMDSC treatment group divided by percentile of mMDSC Sham group). N=3 (3 independent experiments with 2-3 mice pooled).

S1 Figure: Gating strategy for FACS-based population isolation. Neutrophils were sorted from lung digests as live, singlets, $CD45^{+}$, non-lymphocytes, $Ly6C^{+}$ and $Ly6G^{+}$. Three monocyte/macrophage populations were sorted from lung digests as live, singlets, $CD45^{+}$, non-lymphocytes, $Ly6C^{-}$and $Ly6G^{-}$, and identified as separate populations with variable expression of CD11b and CD11c as: (1) macrophages ($CD11c^{high}$, $CD11b^{variable}$), (2) monocytes-macrophages ($CD11c^{intermediate}$,$CD11b^{high}$), and (3) monocytes ($CD11c^{-}$, $CD11b^{high}$).

S2 Figure: Gating strategy for posthoc analysis of myeloid-derived suppressor cells (MDSCs). Granulocytic (g) MDSCs were identified as live, singlets, $CD45^{+}$, non-lymphocytes that were $Ly6C^{+}$ $Ly6G^{+}$ $CD11b^{+}$ SSC^{high}. Whereas, monocytic (m) MDSCs were identified as live, singlets, $CD45^{+}$, non-lymphocytes that were $Ly6G^{-}$ $CD11b^{+}$ $Ly6C^{+}$ SSC^{low}.

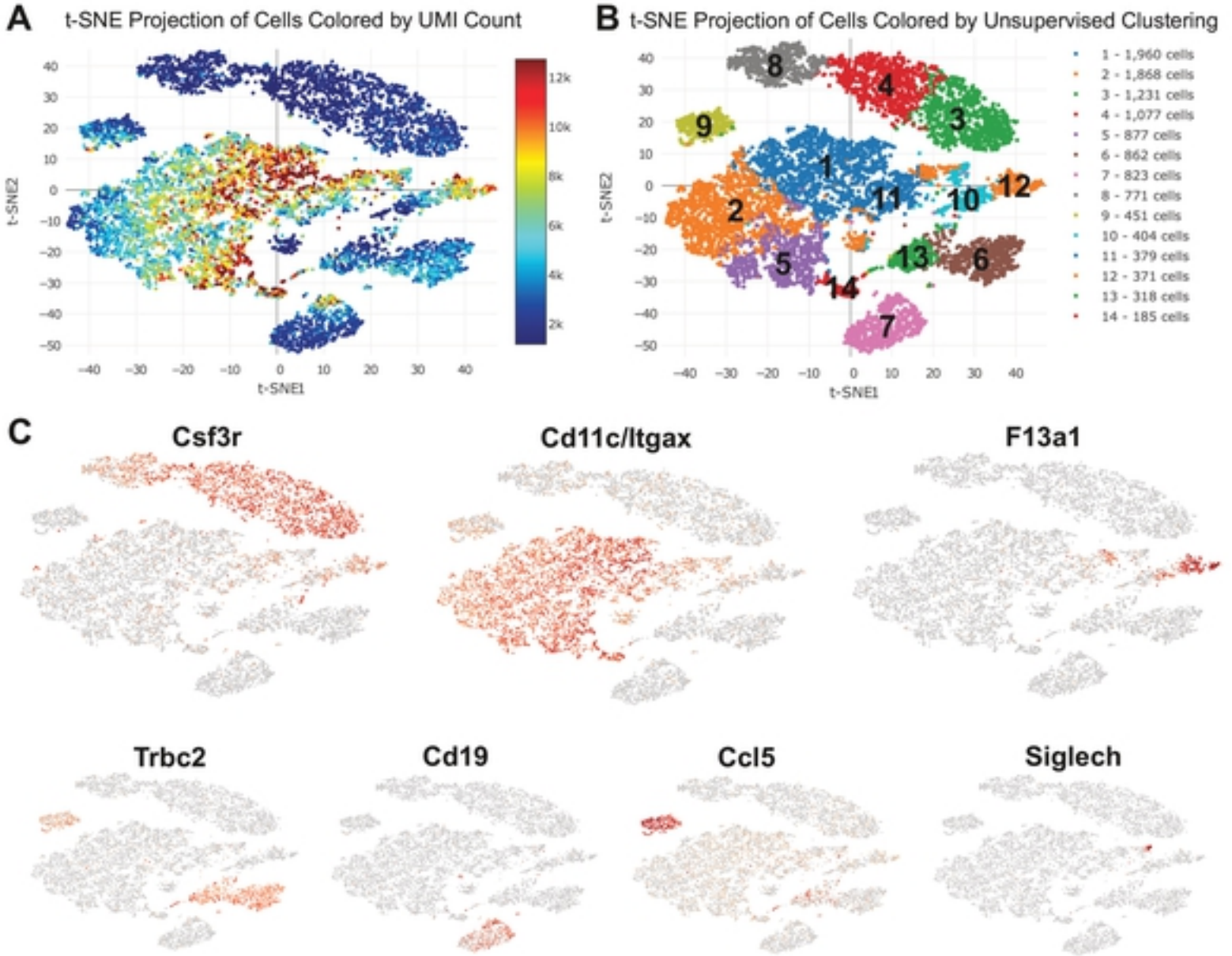
A
t-SNE Projection of Cells Colored by UMI Count
t-SNE2
t-SNE1
12k
10k
8k
6k
4k
2k
B
t-SNE Projection of Cells Colored by Unsupervised Clustering
1 - 1,960 cells
2 - 1,868 cells
3 - 1,231 cells
4 - 1,077 cells
5 - 877 cells
6 - 862 cells
7 - 823 cells
8 - 771 cells
9 - 451 cells
10 - 404 cells
11 - 379 cells
12 - 371 cells
13 - 318 cells
14 - 185 cells
C
Csf3r
Cd11c/Itgax
F13a1
Trbc2
Cd19
Ccl5
Siglech

Figure 1

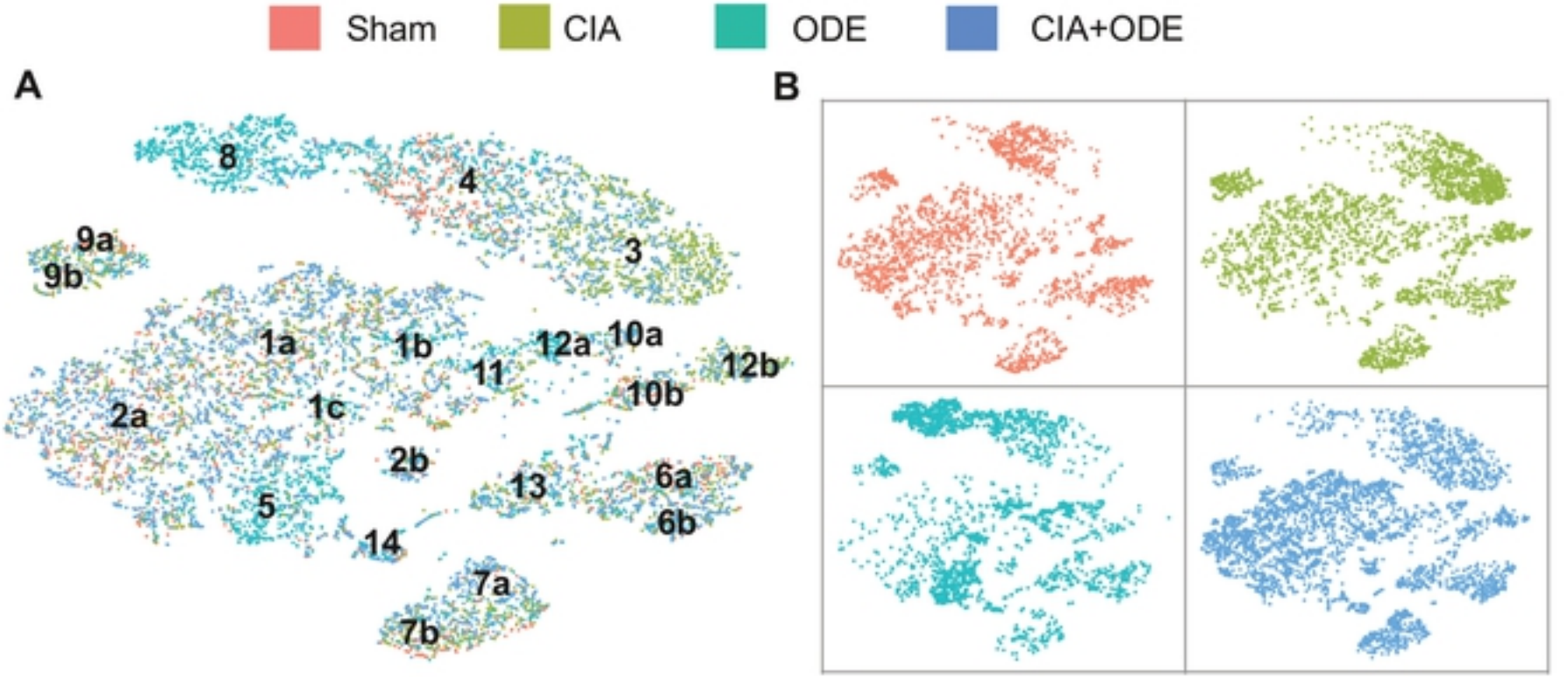
Sham
CIA
ODE
CIA+ODE
A
B
8
4
3
9a
9b
1a
1b
12a
10a
12b
11
10b
1c
2a
2b
13
6a
6b
5
14
7a
7b

Figure 2

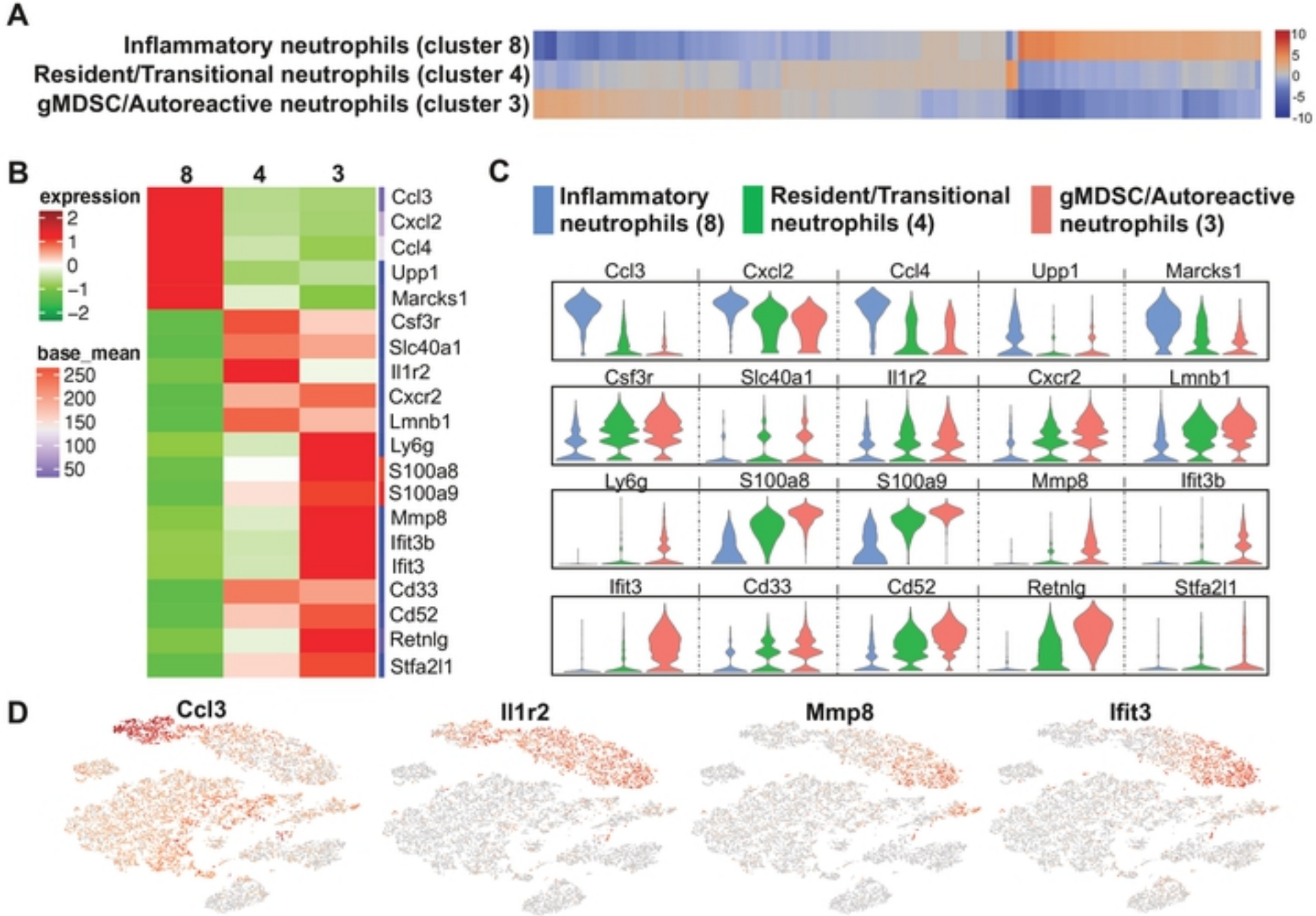
A
Inflammatory neutrophils (cluster 8)
Resident/Transitional neutrophils (cluster 4)
gMDSC/Autoreactive neutrophils (cluster 3)
10
5
0
-5
-10
B
8
4
3
expression
2
1
0
−1
−2
base_mean
250
200
150
100
50
Ccl3
Cxcl2
Ccl4
Upp1
Marcks1
Csf3r
Slc40a1
Il1r2
Cxcr2
Lmnb1
Ly6g
S100a8
S100a9
Mmp8
Ifit3b
Ifit3
Cd33
Cd52
Retnlg
Stfa2l1
C
Inflammatory neutrophils (8)
Resident/Transitional neutrophils (4)
gMDSC/Autoreactive neutrophils (3)
Ccl3
Cxcl2
Ccl4
Upp1
Marcks1
Csf3r
Slc40a1
Il1r2
Cxcr2
Lmnb1
Ly6g
S100a8
S100a9
Mmp8
Ifit3b
Ifit3
Cd33
Cd52
Retnlg
Stfa2l1
D
Ccl3
Il1r2
Mmp8
Ifit3

Figure 3

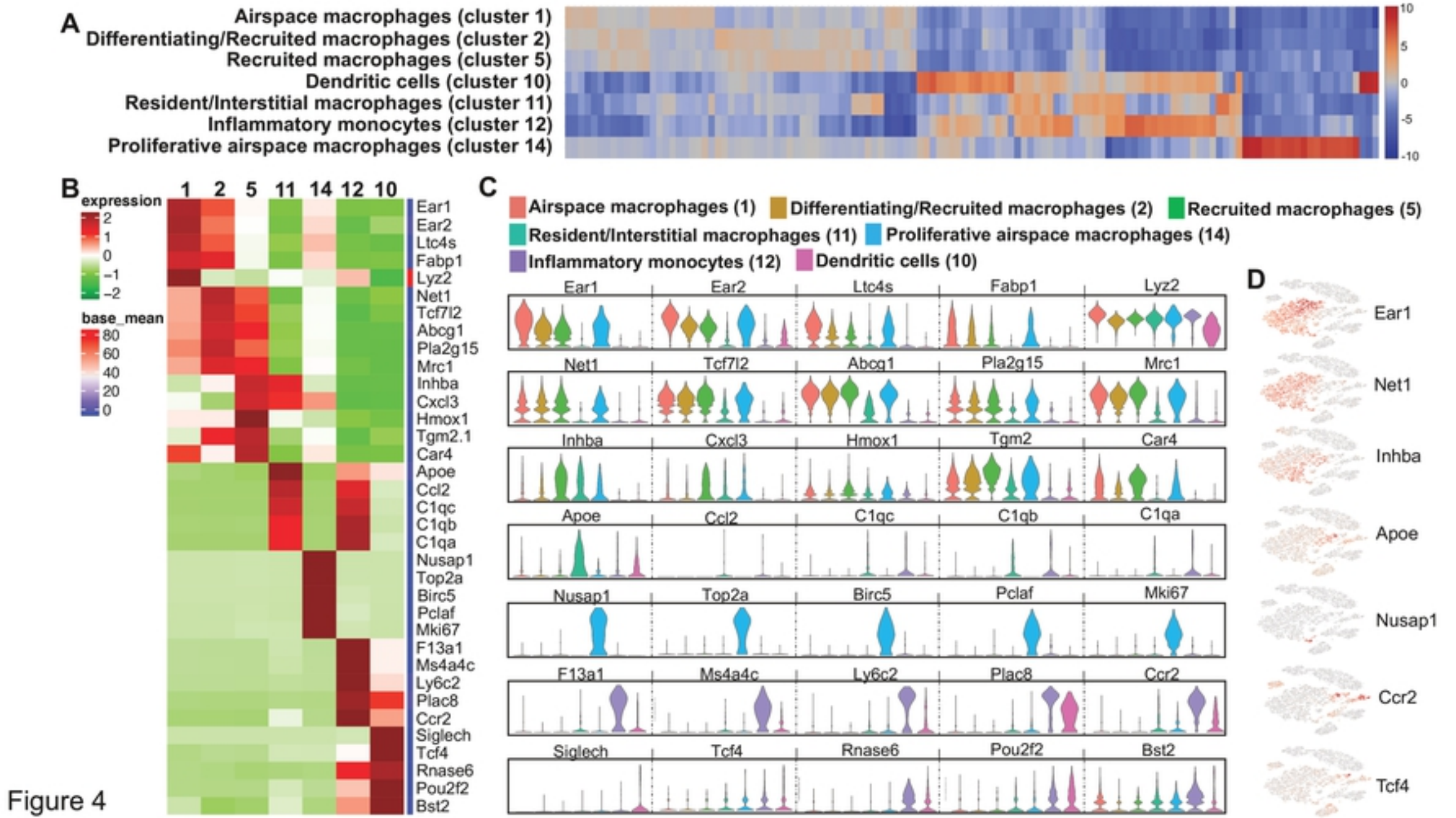
A
Airspace macrophages (cluster 1)
Differentiating/Recruited macrophages (cluster 2)
Recruited macrophages (cluster 5)
Dendritic cells (cluster 10)
Resident/Interstitial macrophages (cluster 11)
Inflammatory monocytes (cluster 12)
Proliferative airspace macrophages (cluster 14)
10
5
0
-5
-10
B
1 2 5 11 14 12 10
expression
2
1
0
−1
−2
base_mean
80
60
40
20
0
Ear1
Ear2
Ltc4s
Fabp1
Lyz2
Net1
Tcf7l2
Abcg1
Pla2g15
Mrc1
Inhba
Cxcl3
Hmox1
Tgm2.1
Car4
Apoe
Ccl2
C1qc
C1qb
C1qa
Nusap1
Top2a
Birc5
Pclaf
Mki67
F13a1
Ms4a4c
Ly6c2
Plac8
Ccr2
Siglech
Tcf4
Rnase6
Pou2f2
Bst2
C
Airspace macrophages (1)
Differentiating/Recruited macrophages (2)
Recruited macrophages (5)
Resident/Interstitial macrophages (11)
Proliferative airspace macrophages (14)
Inflammatory monocytes (12)
Dendritic cells (10)
Ear1
Ear2
Ltc4s
Fabp1
Lyz2
Net1
Tcf7l2
Abcg1
Pla2g15
Mrc1
Inhba
Cxcl3
Hmox1
Tgm2
Car4
Apoe
Ccl2
C1qc
C1qb
C1qa
Nusap1
Top2a
Birc5
Pclaf
Mki67
F13a1
Ms4a4c
Ly6c2
Plac8
Ccr2
Siglech
Tcf4
Rnase6
Pou2f2
Bst2
D
Ear1
Net1
Inhba
Apoe
Nusap1
Ccr2
Tcf4

Figure 4

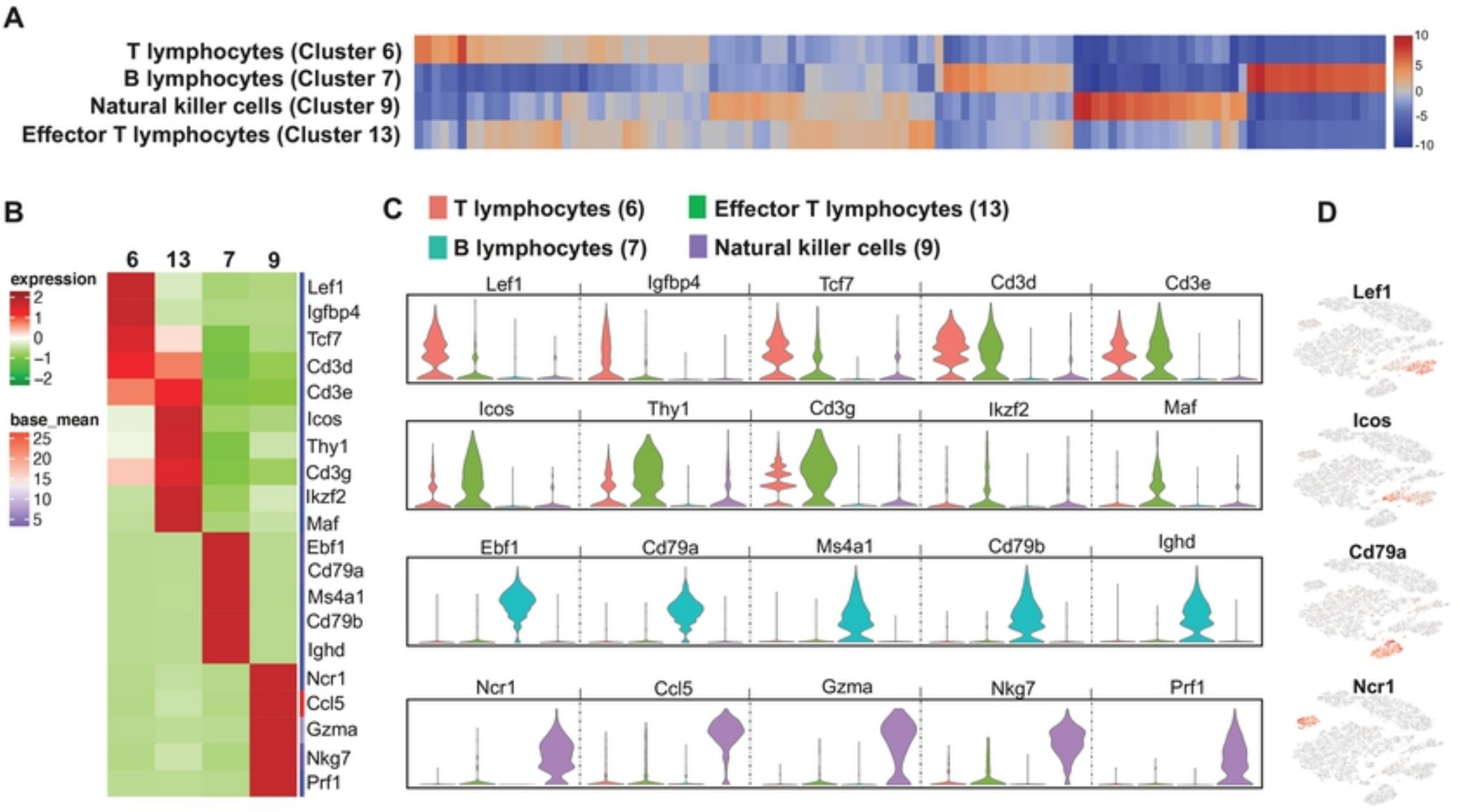
A
T lymphocytes (Cluster 6)
B lymphocytes (Cluster 7)
Natural killer cells (Cluster 9)
Effector T lymphocytes (Cluster 13)
10
5
0
-5
-10
B
6
13
7
9
expression
2
1
0
−1
−2
base_mean
25
20
15
10
5
Lef1
Igfbp4
Tcf7
Cd3d
Cd3e
Icos
Thy1
Cd3g
Ikzf2
Maf
Ebf1
Cd79a
Ms4a1
Cd79b
Ighd
Ncr1
Ccl5
Gzma
Nkg7
Prf1
C
T lymphocytes (6)
Effector T lymphocytes (13)
B lymphocytes (7)
Natural killer cells (9)
Lef1
Igfbp4
Tcf7
Cd3d
Cd3e
Icos
Thy1
Cd3g
Ikzf2
Maf
Ebf1
Cd79a
Ms4a1
Cd79b
Ighd
Ncr1
Ccl5
Gzma
Nkg7
Prf1
D
Lef1
Icos
Cd79a
Ncr1

Figure 5

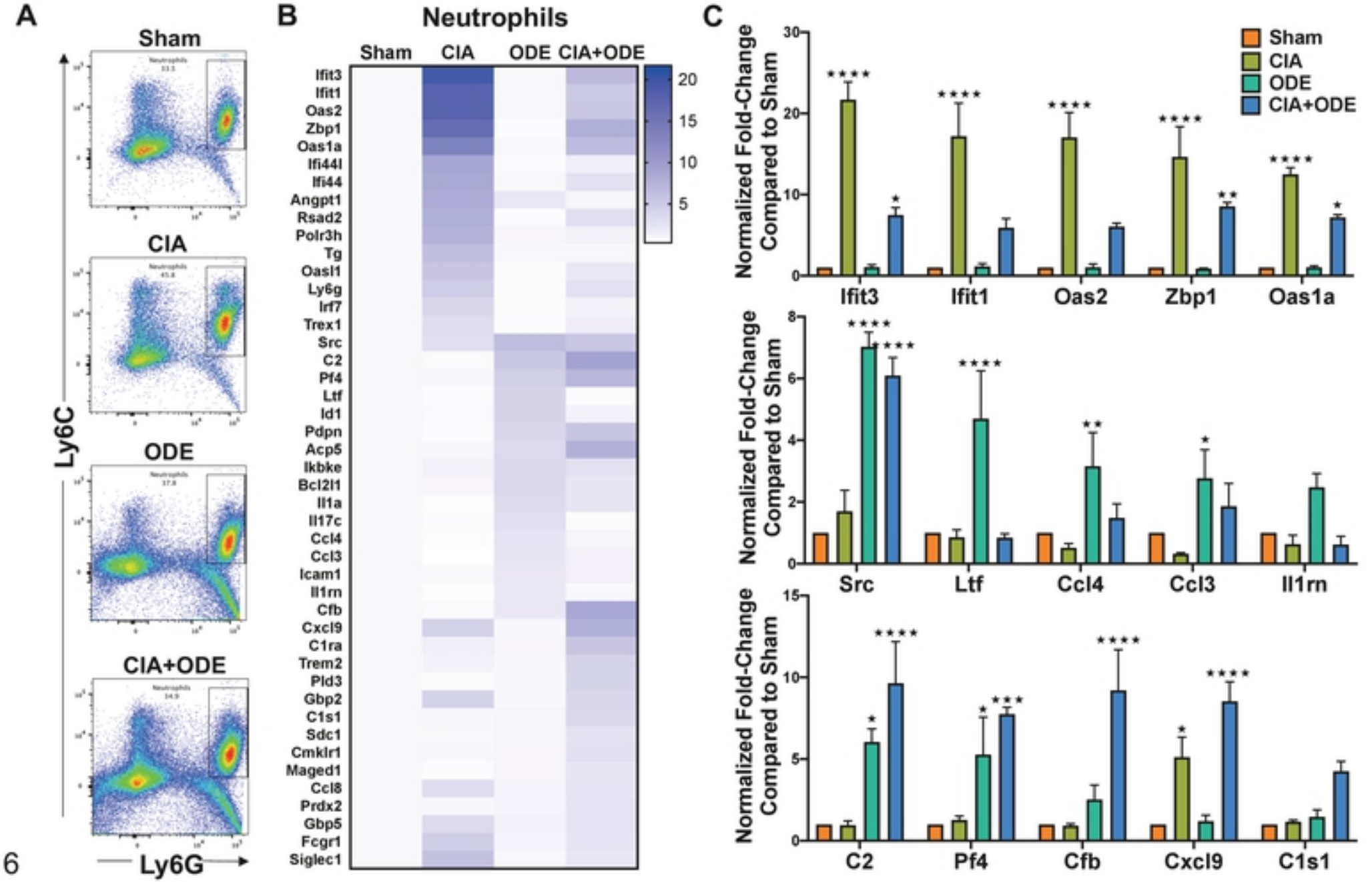
A
Sham
CIA
ODE
CIA+ODE
Ly6C
Ly6G
B
Neutrophils
Sham
CIA
ODE
CIA+ODE
Ifit3
Ifit1
Oas2
Zbp1
Oas1a
Ifi44l
Ifi44
Angpt1
Rsad2
Polr3h
Tg
Oasl1
Ly6g
Irf7
Trex1
Src
C2
Pf4
Ltf
Id1
Pdpn
Acp5
Ikbke
Bcl2l1
Il1a
Il17c
Ccl4
Ccl3
Icam1
Il1rn
Cfb
Cxcl9
C1ra
Trem2
Pld3
Gbp2
C1s1
Sdc1
Cmklr1
Maged1
Ccl8
Prdx2
Gbp5
Fcgr1
Siglec1
20
15
10
5
C
Sham
CIA
ODE
CIA+ODE
Normalized Fold-Change Compared to Sham
Ifit3
Ifit1
Oas2
Zbp1
Oas1a
Src
Ltf
Ccl4
Ccl3
Il1rn
C2
Pf4
Cfb
Cxcl9
C1s1

Figure 6

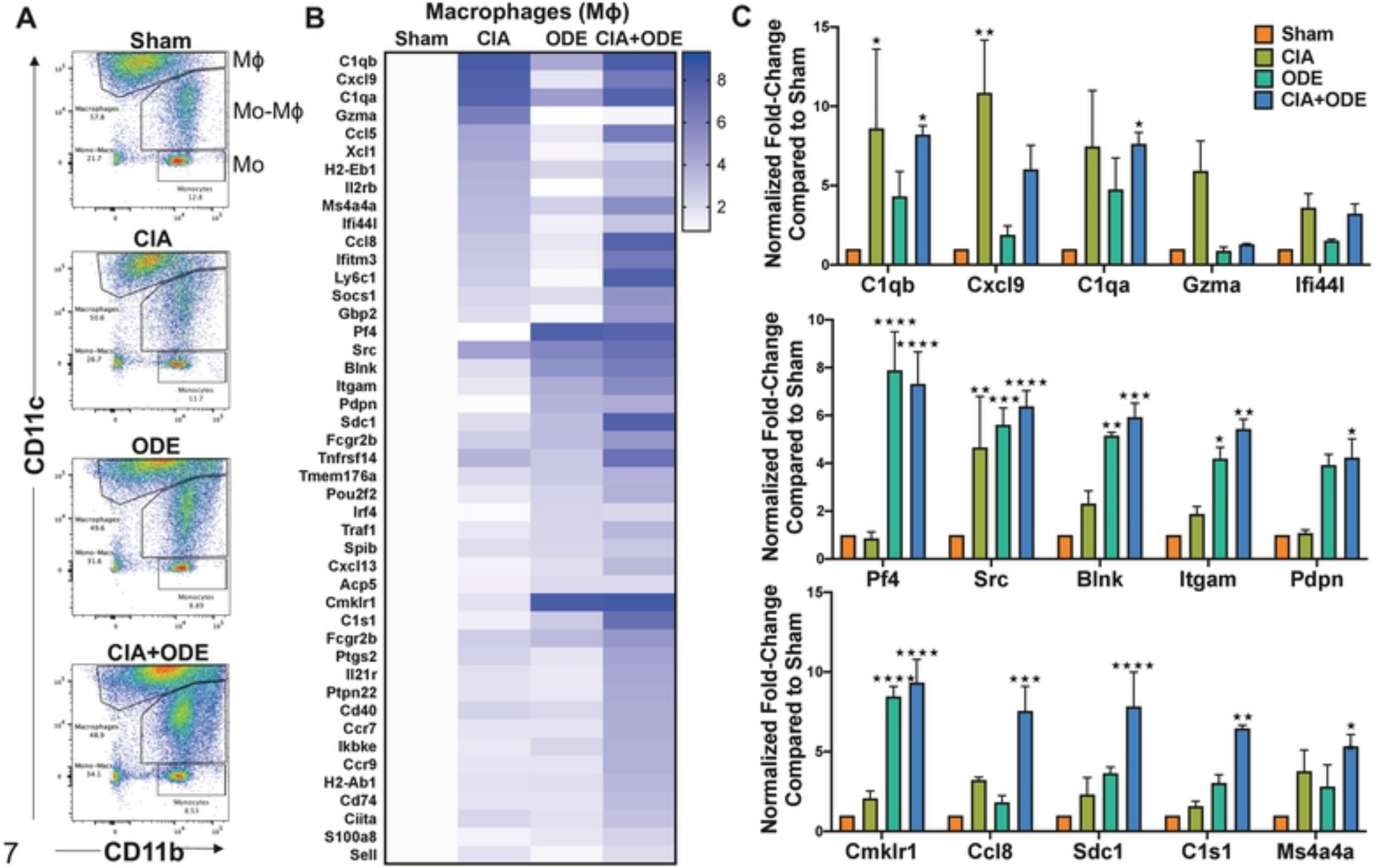
A
Sham
CIA
ODE
CIA+ODE
Mϕ
Mo-Mϕ
Mo
CD11c
CD11b
B
Macrophages (Mϕ)
Sham
CIA
ODE
CIA+ODE
C1qb
Cxcl9
C1qa
Gzma
Ccl5
Xcl1
H2-Eb1
Il2rb
Ms4a4a
Ifi44l
Ccl8
Ifitm3
Ly6c1
Socs1
Gbp2
Pf4
Src
Blnk
Itgam
Pdpn
Sdc1
Fcgr2b
Tnfrsf14
Tmem176a
Pou2f2
Irf4
Traf1
Spib
Cxcl13
Acp5
Cmklr1
C1s1
Fcgr2b
Ptgs2
Il21r
Ptpn22
Cd40
Ccr7
Ikbke
Ccr9
H2-Ab1
Cd74
Ciita
S100a8
Sell
8
6
4
2
C
Sham
CIA
ODE
CIA+ODE
Normalized Fold-Change Compared to Sham
C1qb
Cxcl9
C1qa
Gzma
Ifi44l
Pf4
Src
Blnk
Itgam
Pdpn
Cmklr1
Ccl8
Sdc1
C1s1
Ms4a4a

Figure 7

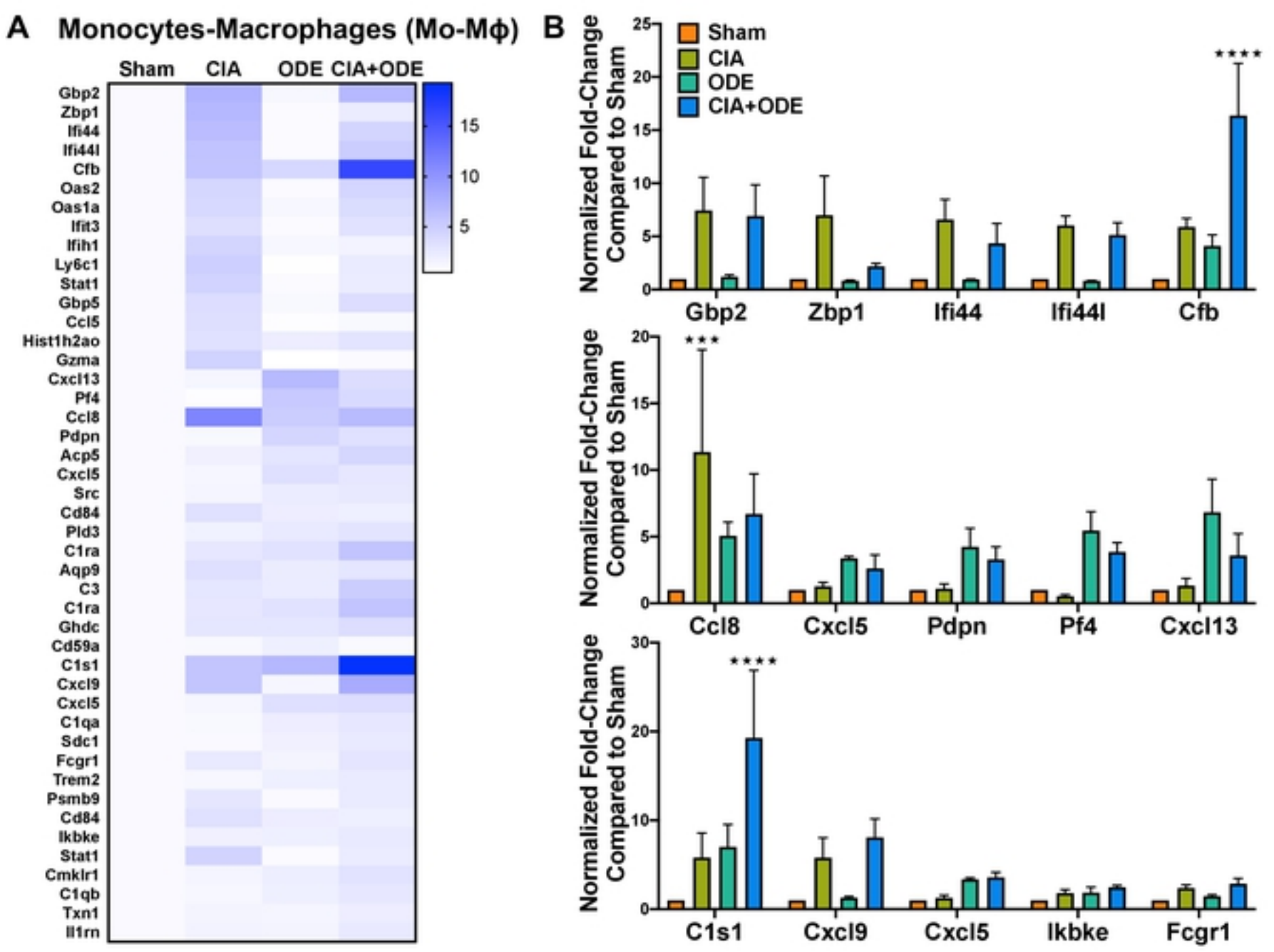
A
Monocytes-Macrophages (Mo-Mϕ)
Sham
CIA
ODE
CIA+ODE
Gbp2
Zbp1
Ifi44
Ifi44l
Cfb
Oas2
Oas1a
Ifit3
Ifih1
Ly6c1
Stat1
Gbp5
Ccl5
Hist1h2ao
Gzma
Cxcl13
Pf4
Ccl8
Pdpn
Acp5
Cxcl5
Src
Cd84
Pld3
C1ra
Aqp9
C3
C1ra
Ghdc
Cd59a
C1s1
Cxcl9
Cxcl5
C1qa
Sdc1
Fcgr1
Trem2
Psmb9
Cd84
Ikbke
Stat1
Cmklr1
C1qb
Txn1
Il1rn
15
10
5
B
Sham
CIA
ODE
CIA+ODE
Normalized Fold-Change Compared to Sham
****
Gbp2
Zbp1
Ifi44
Ifi44l
Cfb
***
Ccl8
Cxcl5
Pdpn
Pf4
Cxcl13
****
C1s1
Cxcl9
Cxcl5
Ikbke
Fcgr1

Figure 8

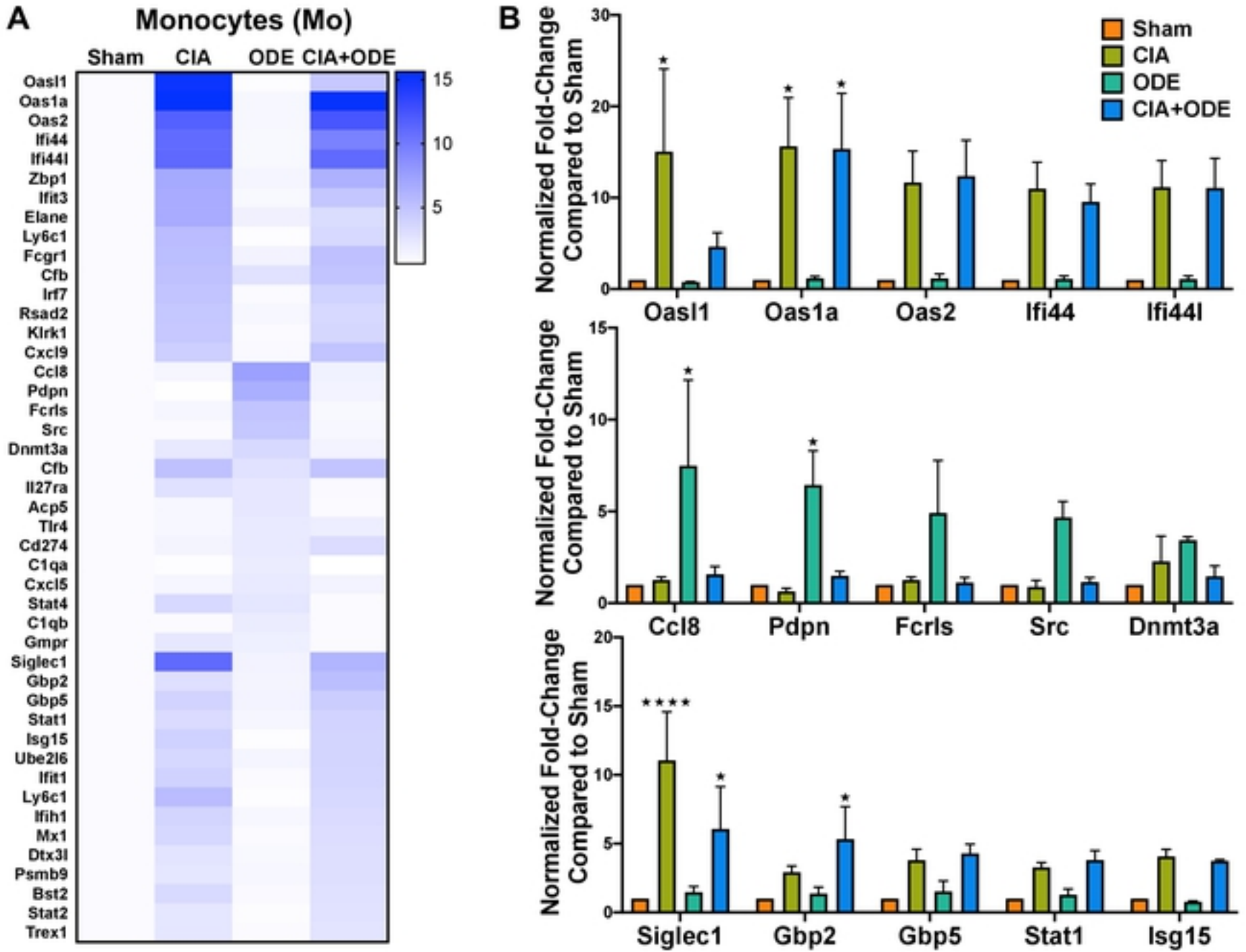
A
Monocytes (Mo)
Sham
CIA
ODE
CIA+ODE
Oasl1
Oas1a
Oas2
Ifi44
Ifi44l
Zbp1
Ifit3
Elane
Ly6c1
Fcgr1
Cfb
Irf7
Rsad2
Klrk1
Cxcl9
Ccl8
Pdpn
Fcrls
Src
Dnmt3a
Cfb
Il27ra
Acp5
Tlr4
Cd274
C1qa
Cxcl5
Stat4
C1qb
Gmpr
Siglec1
Gbp2
Gbp5
Stat1
Isg15
Ube2l6
Ifit1
Ly6c1
Ifih1
Mx1
Dtx3l
Psmb9
Bst2
Stat2
Trex1
15
10
5
B
Sham
CIA
ODE
CIA+ODE
Normalized Fold-Change Compared to Sham
Oasl1
Oas1a
Oas2
Ifi44
Ifi44l
Ccl8
Pdpn
Fcrls
Src
Dnmt3a
Siglec1
Gbp2
Gbp5
Stat1
Isg15

Figure 9

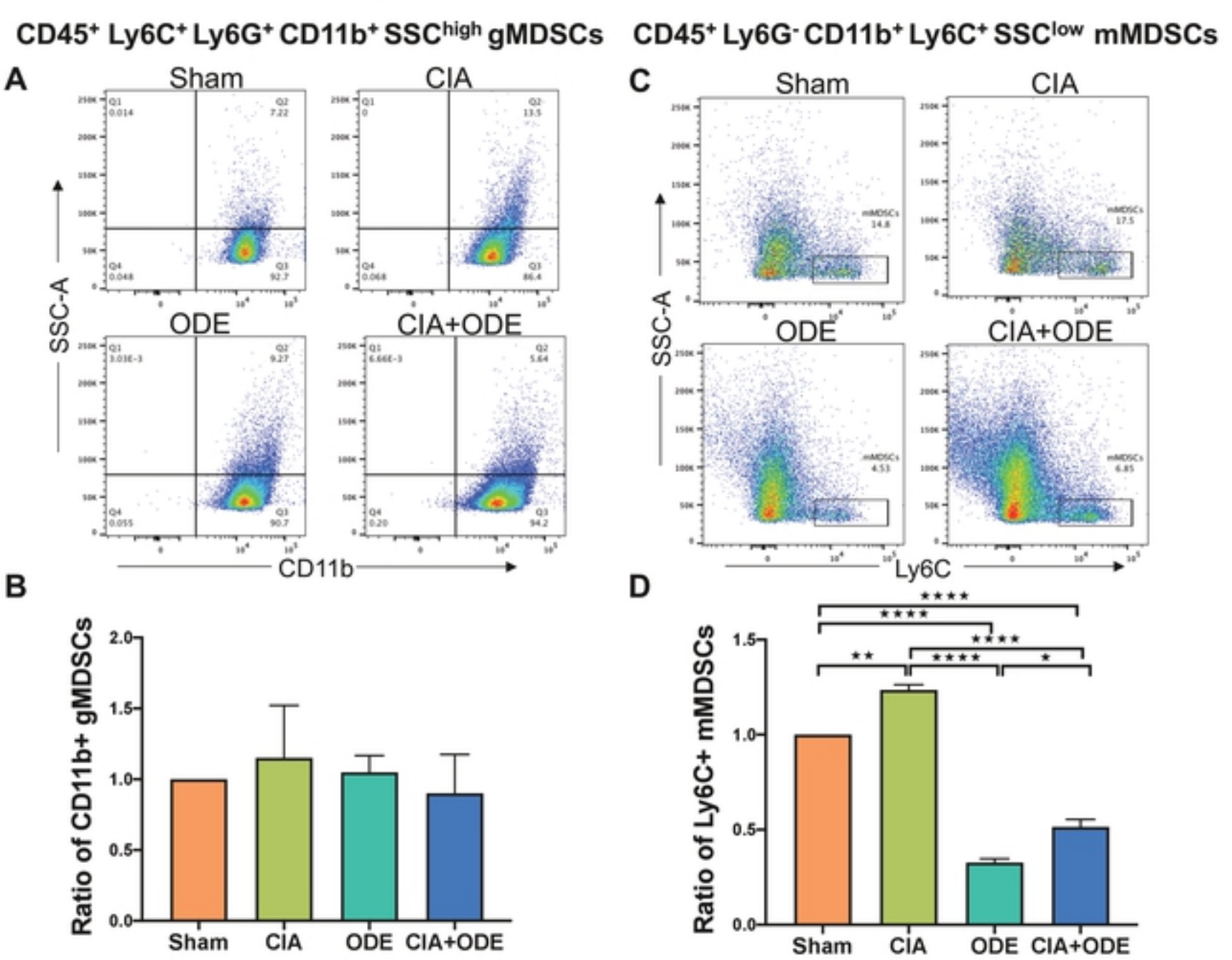
CD45+ Ly6C+ Ly6G+ CD11b+ SSChigh gMDSCs
CD45+ Ly6G- CD11b+ Ly6C+ SSClow mMDSCs
A
Sham
CIA
ODE
CIA+ODE
SSC-A
CD11b
C
Sham
CIA
ODE
CIA+ODE
SSC-A
Ly6C
B
Ratio of CD11b+ gMDSCs
Sham
CIA
ODE
CIA+ODE
D
Ratio of Ly6C+ mMDSCs
Sham
CIA
ODE
CIA+ODE

Figure 10